

## Supporting Information

# Unexpected reactivity of cyclometalated iridium(III) dimers. Direct synthesis of a mononuclear luminescent complex

Jing Tu,<sup>a</sup> Daniele Veclani,<sup>b</sup> Filippo Monti,<sup>\*b</sup> Andrea Mazzanti,<sup>a</sup>  
Letizia Sambri,<sup>a</sup> Nicola Armaroli<sup>b</sup> and Andrea Baschieri<sup>\*b</sup>

<sup>a</sup> Department of Industrial Chemistry "Toso Montanari", University of Bologna, 40136 Bologna, Italy.

<sup>b</sup> Institute for Organic Synthesis and Photoreactivity (ISOF), National Research Council of Italy (CNR), Via Piero Gobetti 101, 40129 Bologna, Italy.

E-mail: F. M.: [filippo.monti@isof.cnr.it](mailto:filippo.monti@isof.cnr.it)  
A. B.: [andrea.baschieri@isof.cnr.it](mailto:andrea.baschieri@isof.cnr.it)

## Table of contents

<i>Contents</i>	<i>Pages</i>
NMR spectra of complexes <b>A</b> and <b>B</b>	S2 – S8
NMR spectra of complexes <b>A</b> and <b>B</b> obtained using alternative synthetic procedures	S9
NMR spectra of the [Ir(ppy) <sub>2</sub> (μ-OH)] <sub>2</sub> dimer	S10
ESI <sup>+</sup> spectrum of complexes <b>A</b> and <b>B</b>	S11 – S12
X-ray data for compound <b>A</b>	S13 – S22
Optimized structures and DFT data for the reaction mechanism	S23 – S27
Computational, electrochemical and photophysical data	S28 – S33

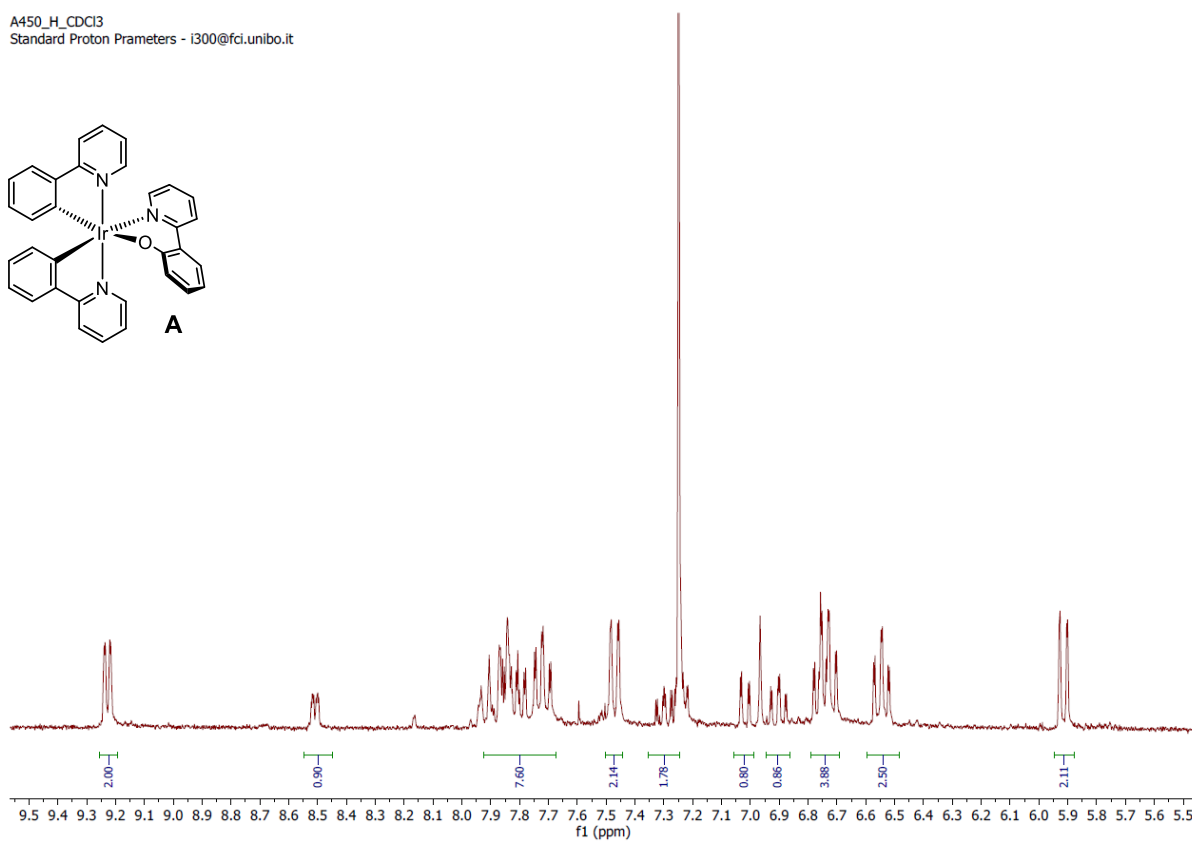
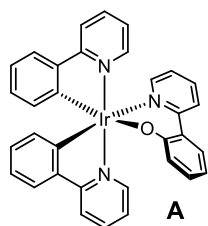


**Fig. S1**  $^1\text{H}$  NMR spectrum of complex **A** in  $\text{CDCl}_3$ .

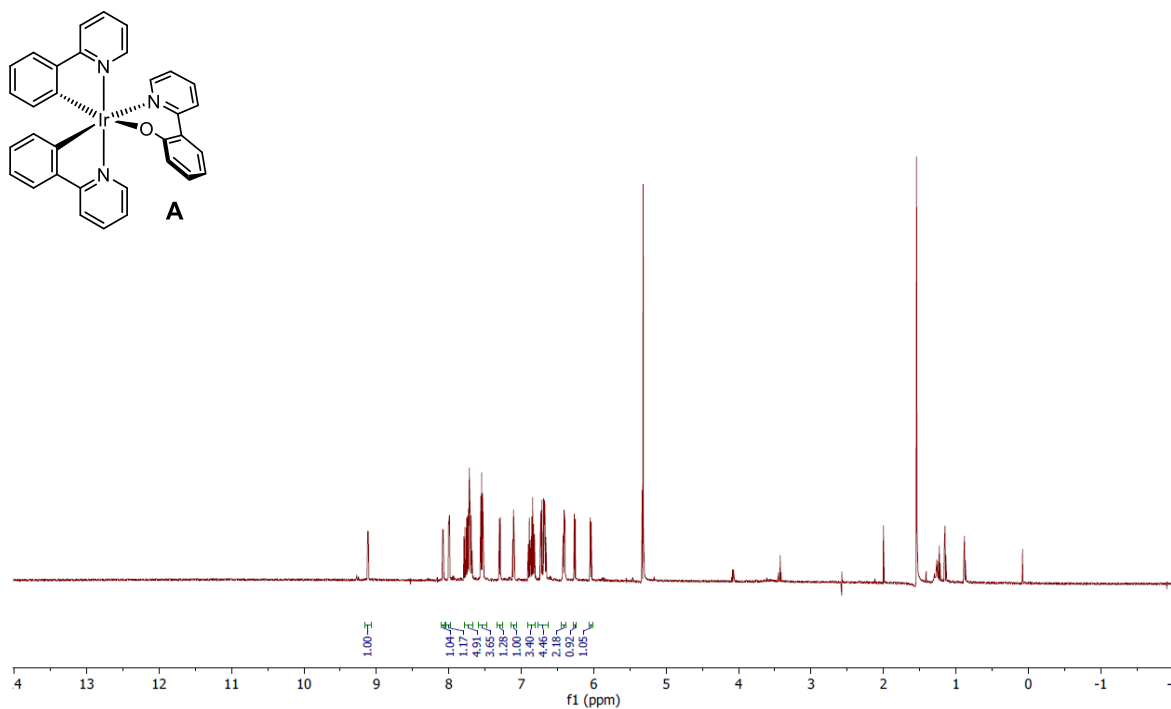


**Fig. S2** <sup>1</sup>H NMR spectrum of complex **A** in CD<sub>2</sub>Cl<sub>2</sub>.

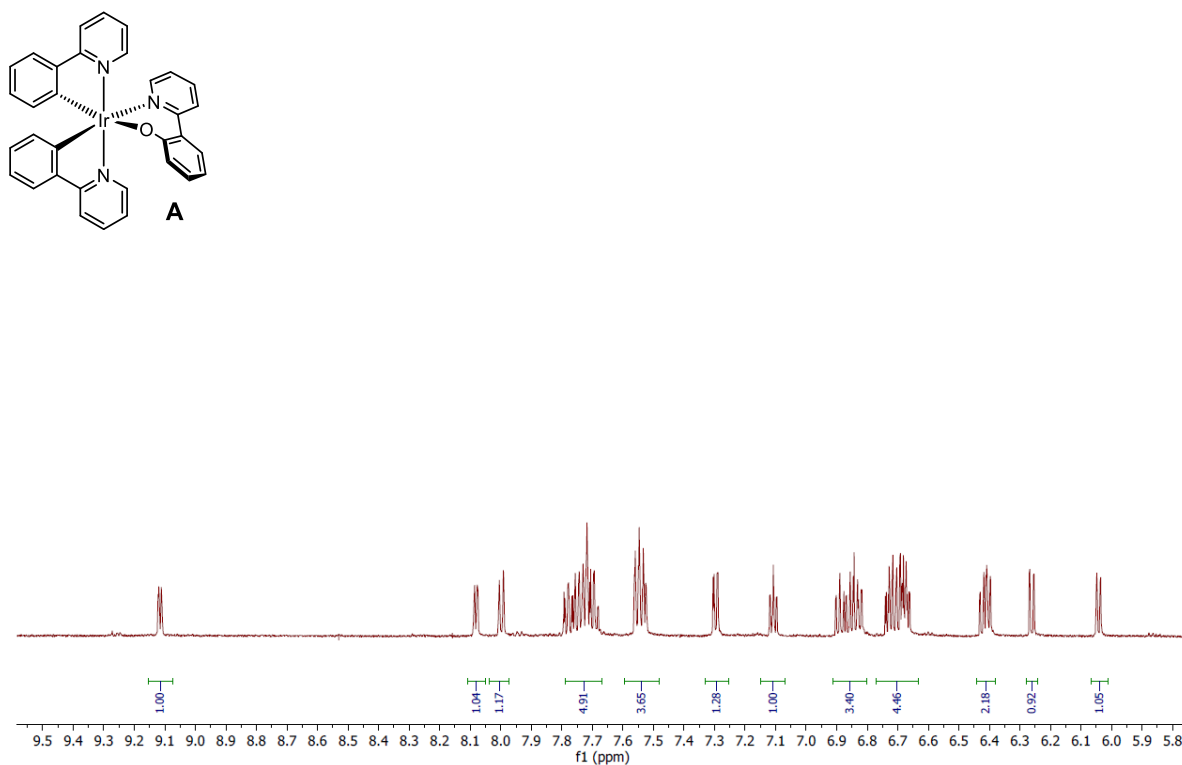


**Fig. S3** Aromatic region of the <sup>1</sup>H NMR spectrum of complex **A** in CD<sub>2</sub>Cl<sub>2</sub>.

Ir-O-fenil-piridina-verde-buono-13C-CD2Cl2-ATB

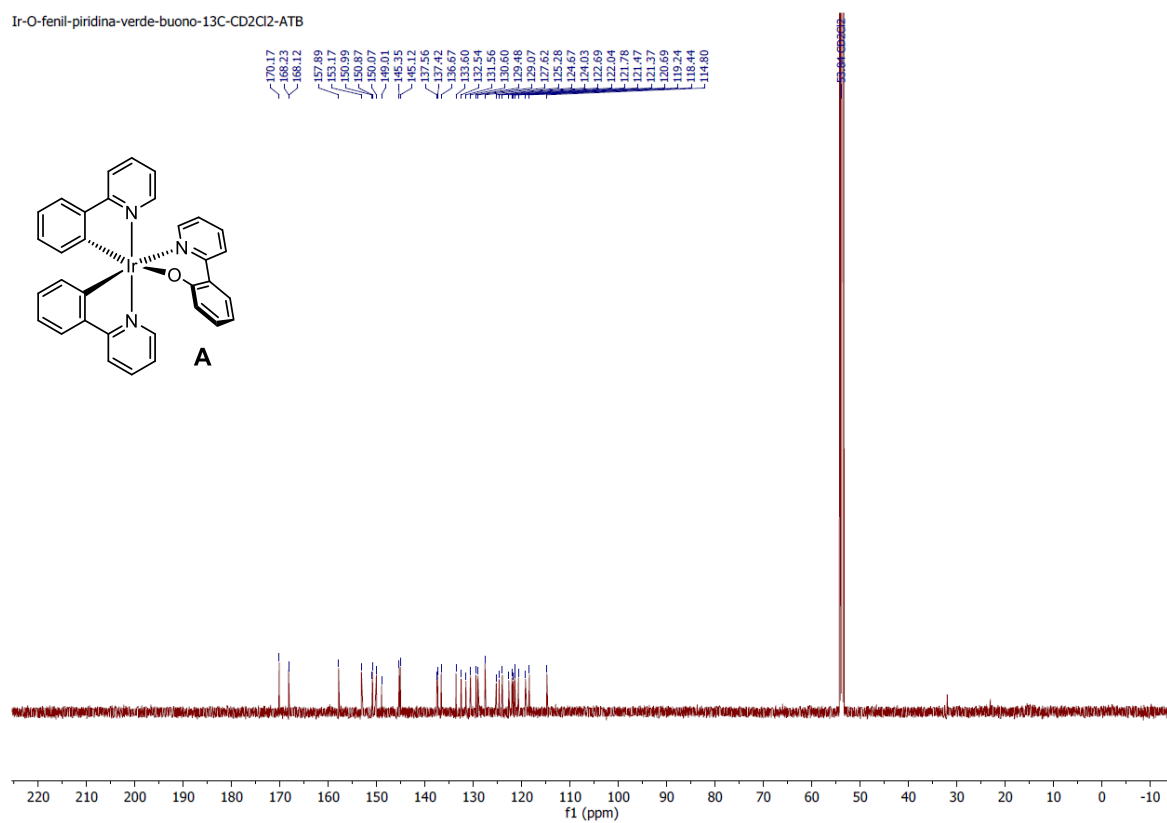


Fig. S4  $^{13}\text{C} \{^1\text{H}\}$  NMR spectrum of complex A in  $\text{CD}_2\text{Cl}_2$ .

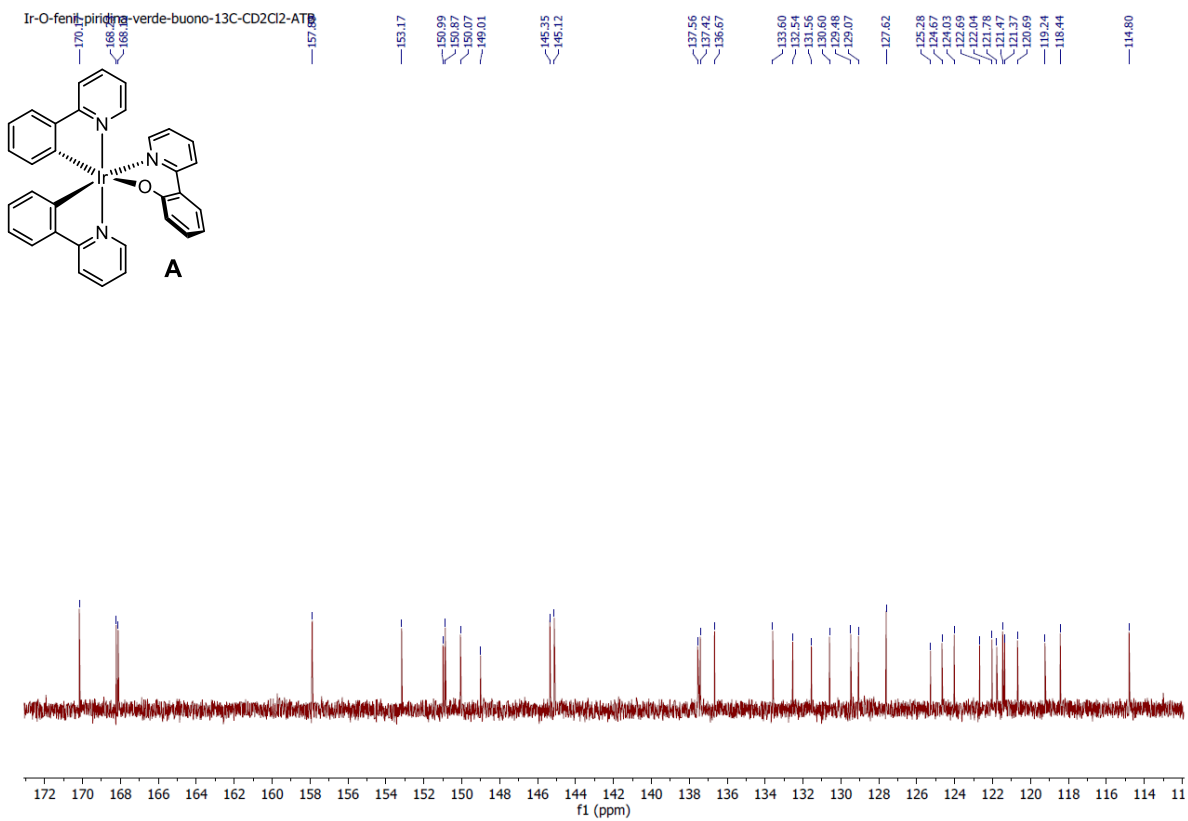
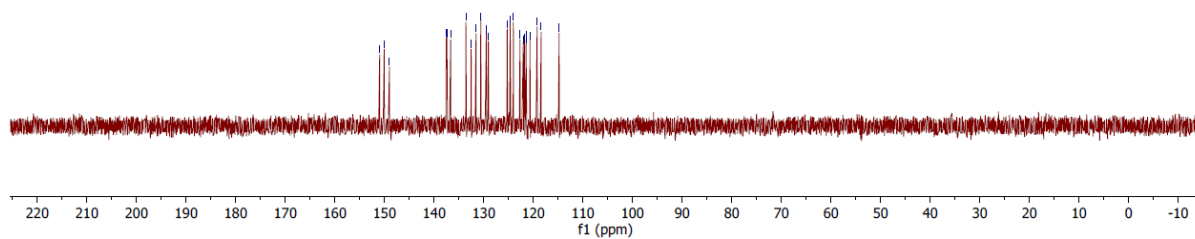
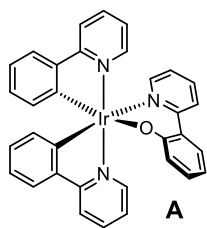


Fig. S5  $^{13}\text{C} \{^1\text{H}\}$  NMR spectrum of complex A in  $\text{CD}_2\text{Cl}_2$ .

Ir-O-fenil-piridina-verde-buono-dept-CD2Cl2-ATB

150.09  
150.07  
148.01  
137.55  
137.41  
136.67  
133.60  
132.54  
132.54  
130.60  
129.48  
129.07  
128.27  
128.67  
128.03  
122.03  
121.78  
121.47  
121.36  
120.69  
118.24  
116.80  
114.80



**Fig. S6** DEPT 135  $\{^1\text{H}\}$  NMR spectrum of complex **A** in  $\text{CD}_2\text{Cl}_2$ .

JTorange-conc\_H\_CDCl3

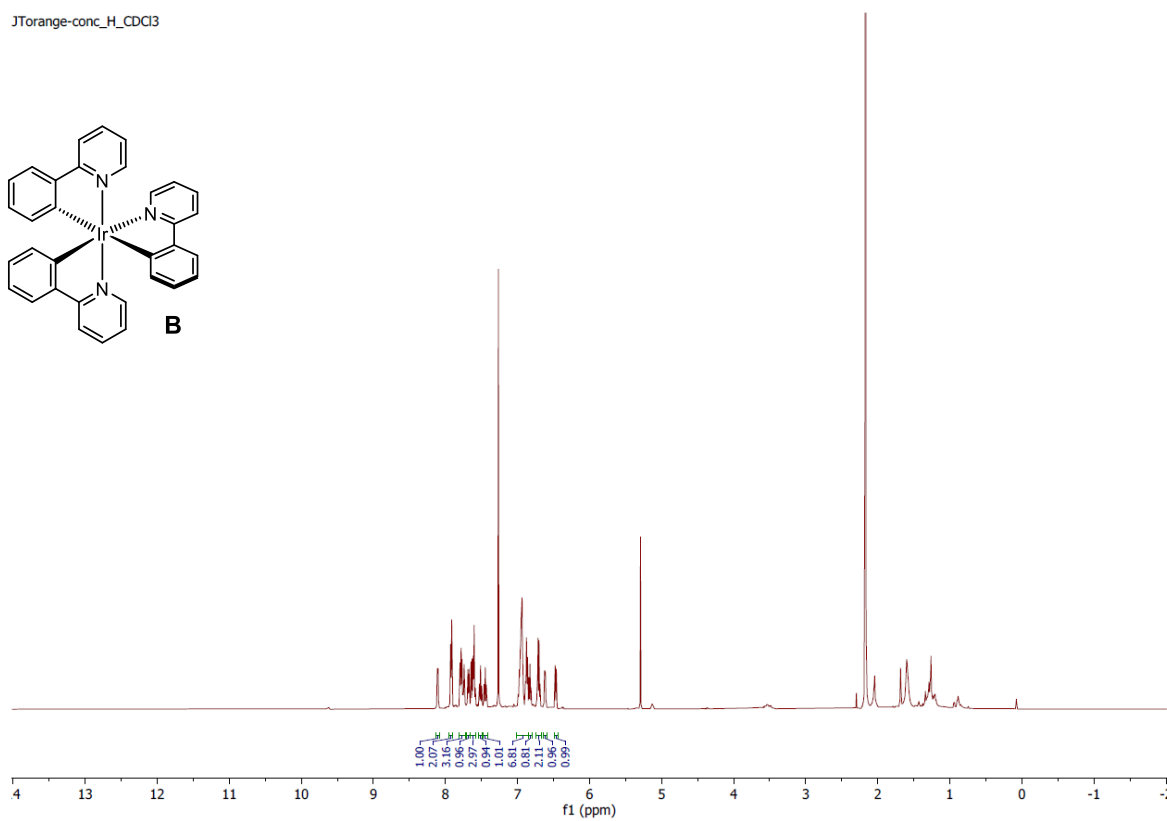
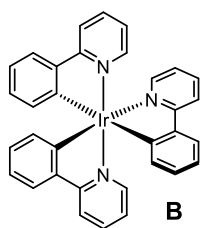


**Fig. S7**  $^1\text{H}$  NMR spectrum of complex **B** in  $\text{CDCl}_3$ .

JTorange-conc\_H\_CDCl3

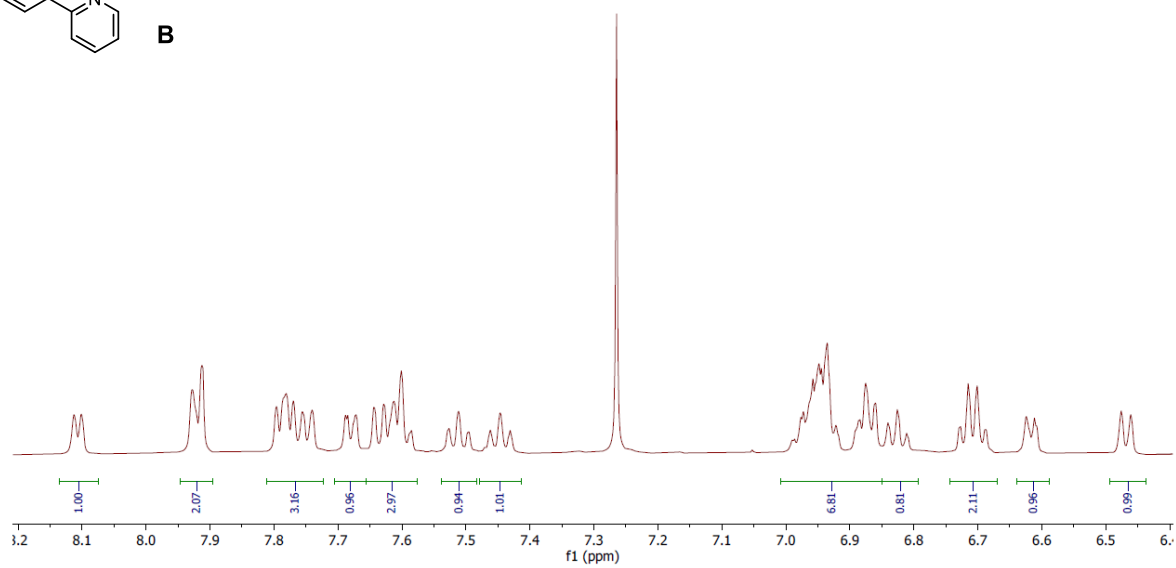
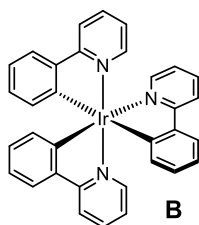


**Fig. S8**  $^1\text{H}$  NMR spectrum of complex **B** in  $\text{CDCl}_3$ .

JTorange-conc\_C-CDCl3

177.78  
176.55  
170.59  
168.52  
167.92  
159.41  
153.25  
151.22  
147.83  
145.32  
144.78  
142.28  
136.43  
135.46  
133.97  
132.75  
130.55  
129.94  
129.54  
124.17  
124.10  
123.91  
122.21  
121.95  
121.18  
118.97  
118.78  
118.54  
118.33

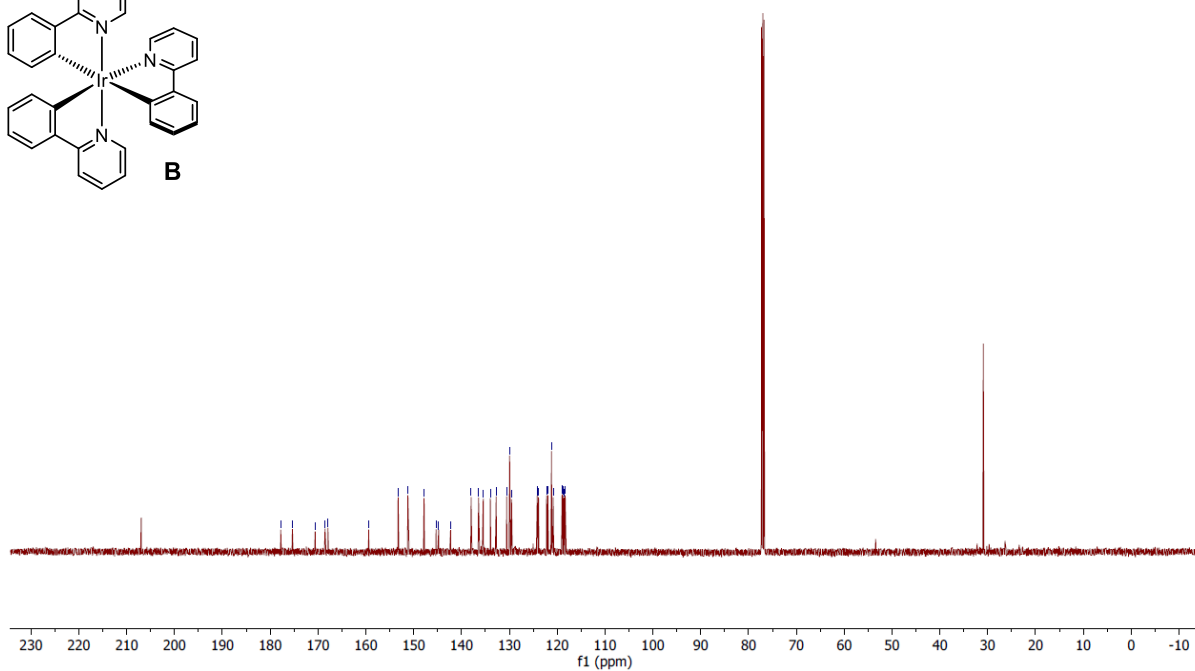
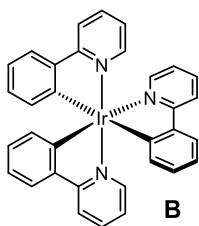


**Fig. S9**  $^{13}\text{C}$   $\{^1\text{H}\}$  NMR spectrum of complex **B** in  $\text{CDCl}_3$ .

JTorange-conc\_C-CDCl3

177.78  
176.55  
170.59  
168.52  
167.92

159.41

153.25

151.22

147.83

145.32

144.78

142.28

137.99

136.43

135.46

133.97

132.75

130.55

129.94

129.54

124.17

124.10

123.91

122.21

121.95

121.18

120.83

118.97

118.78

118.54

118.33

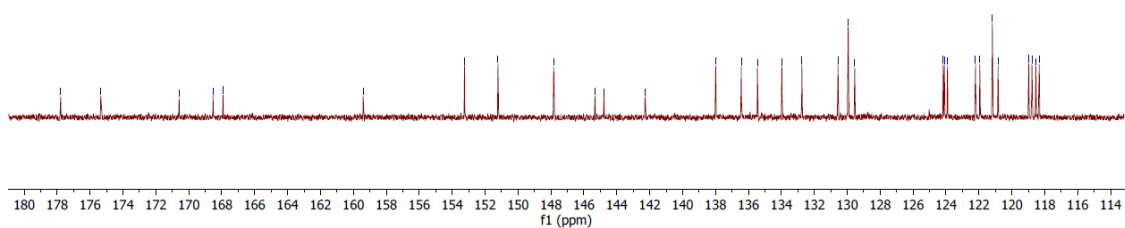
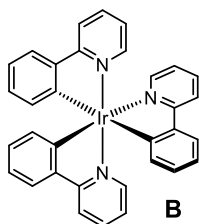


**Fig. S10**  $^{13}\text{C}$   $\{^1\text{H}\}$  NMR spectrum of complex **B** in  $\text{CDCl}_3$ .

JTorange-conc\_DEPT\_CDCl3

153.25  
151.22  
147.83  
137.99  
136.43  
135.46  
133.72  
132.75  
130.55  
129.94  
129.54  
124.17  
124.10  
123.11  
122.21  
121.95  
121.18  
120.83  
118.97  
118.78  
118.44  
118.33

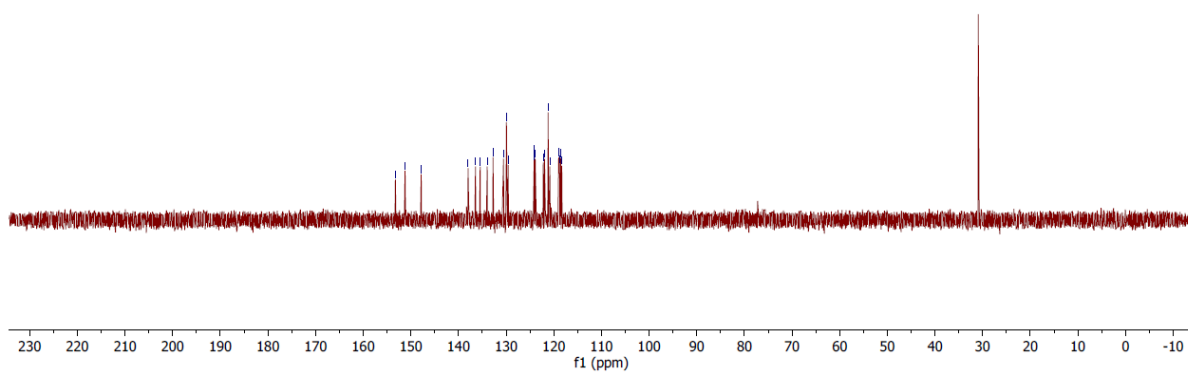
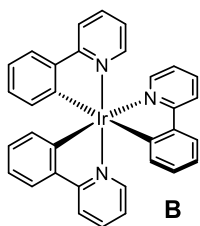


**Fig. S11** DEPT 135  $\{^1\text{H}\}$  NMR spectrum of complex **B** in  $\text{CDCl}_3$ .



JT-A2-col-f2-24h\_H\_CDCl3

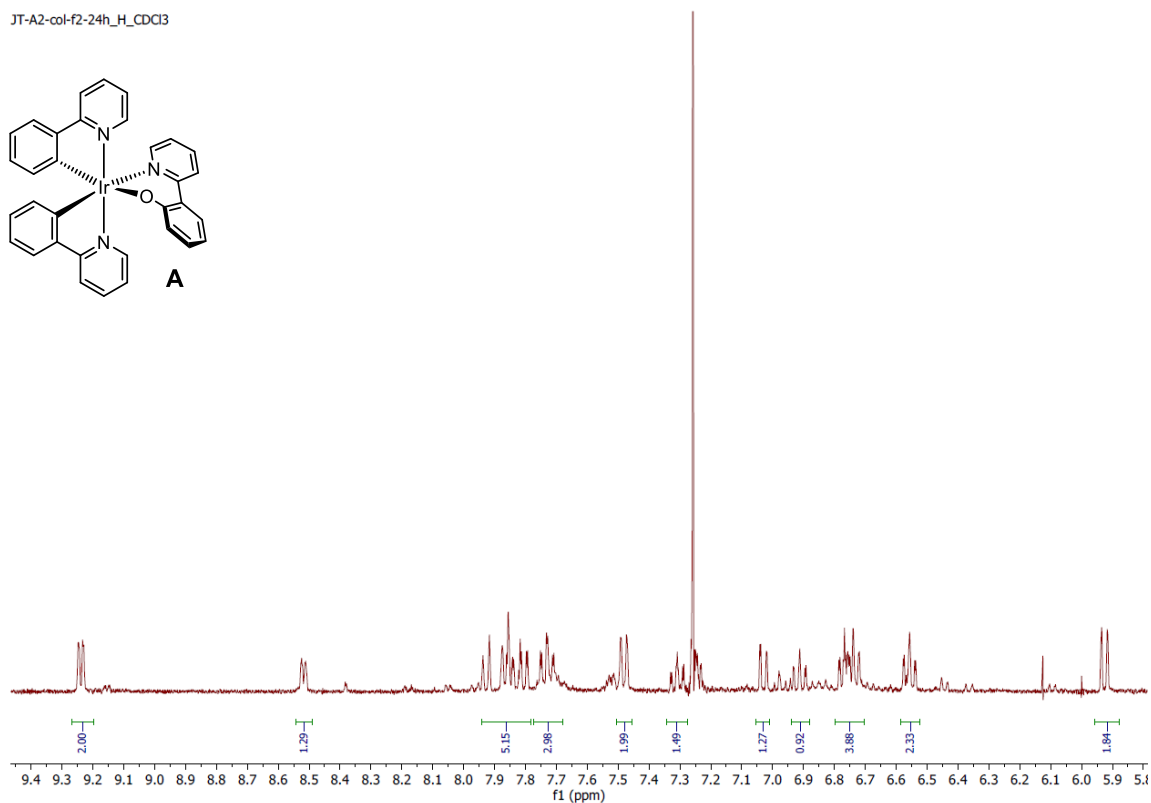
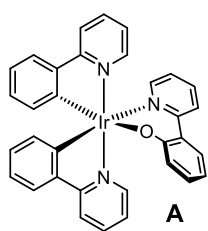


**Fig. S12**  $^1\text{H}$  NMR spectrum of complex **A** in  $\text{CDCl}_3$  synthesized following a method previously reported in the literature and using 2-(*o*-hydroxyphenyl) pyridine as a ligand.

JT47-col-f1\_H\_CDCl3

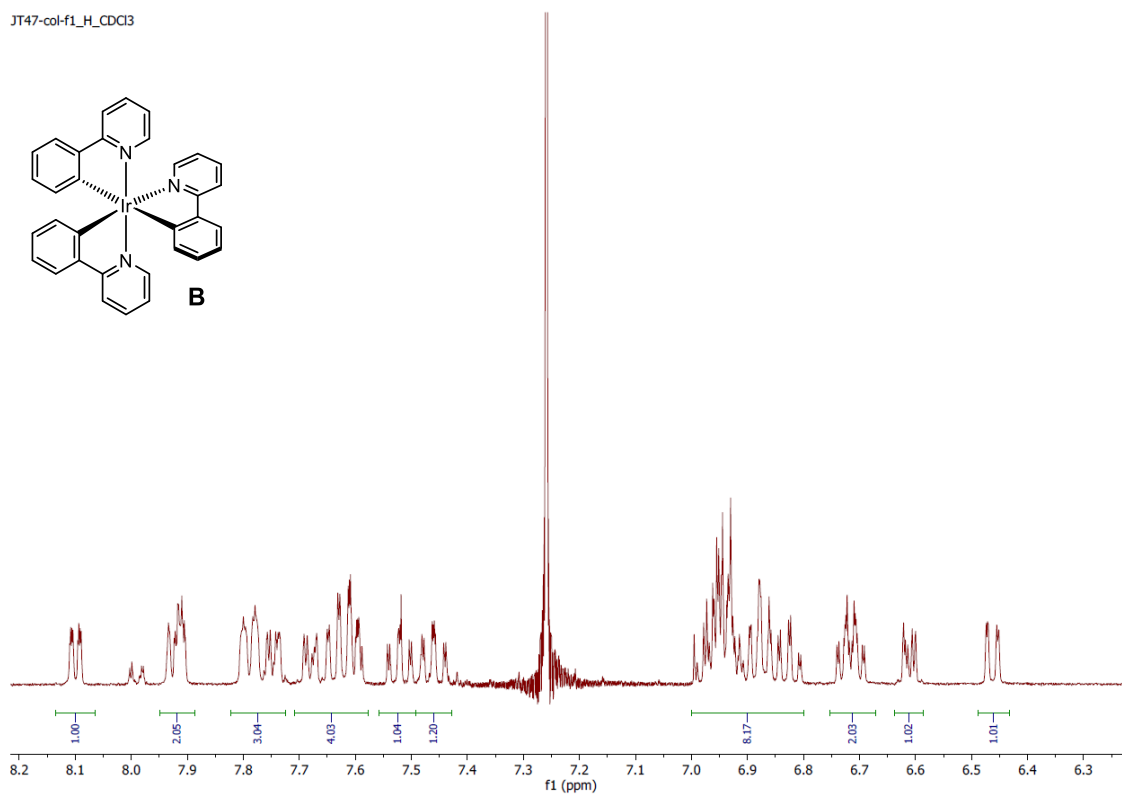
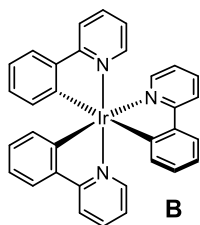


**Fig. S13**  $^1\text{H}$  NMR spectrum of complex **B** in  $\text{CDCl}_3$  synthesized following a method previously reported in the literature and using 2-phenylpyridine as a ligand.

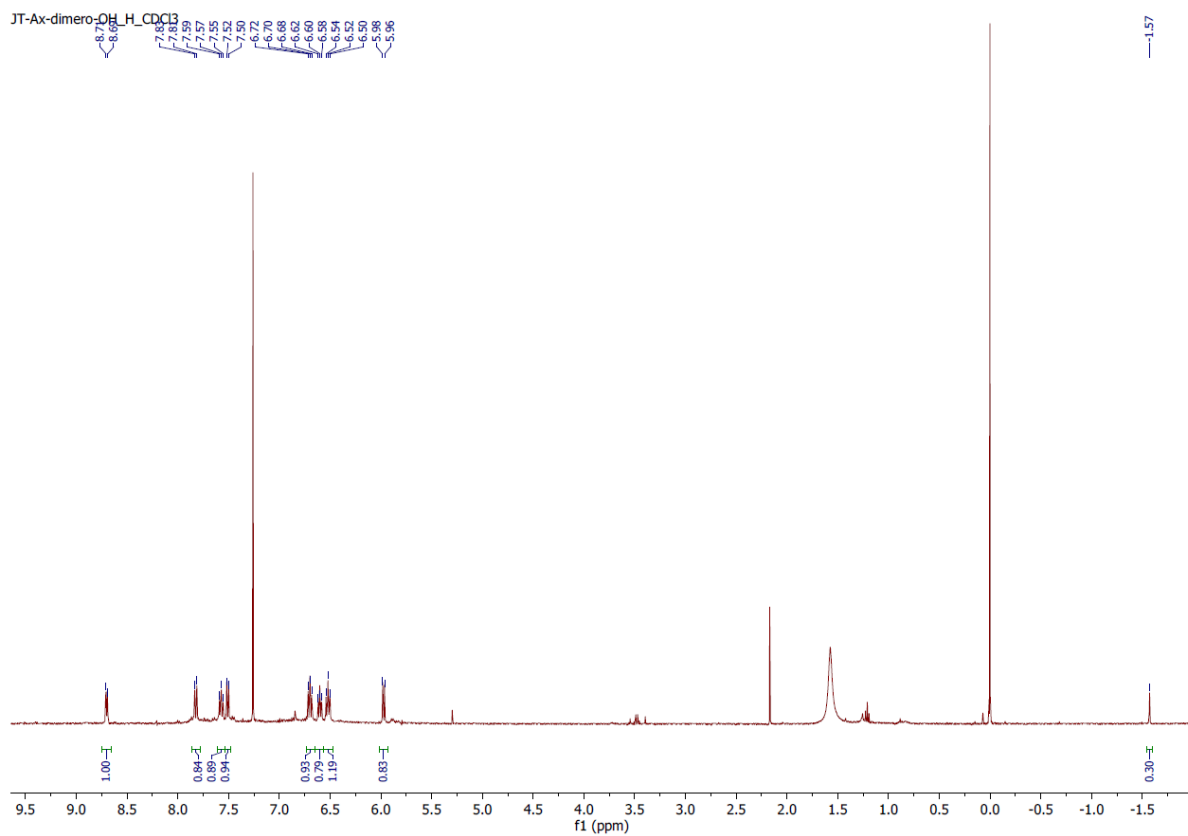


**Fig. S14**  $^1\text{H}$  NMR spectrum of  $[\text{Ir}(\text{ppy})_2(\mu\text{-OH})]_2$  dimer in  $\text{CDCl}_3$  synthesized following a method previously reported in the literature.

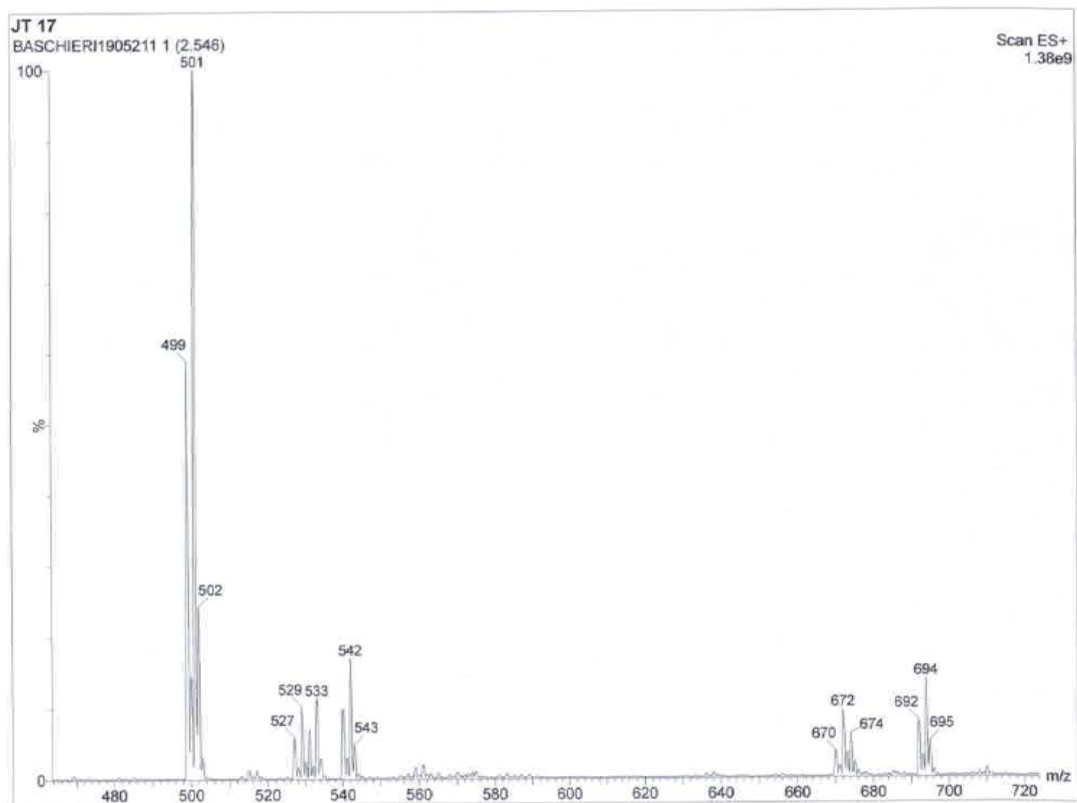
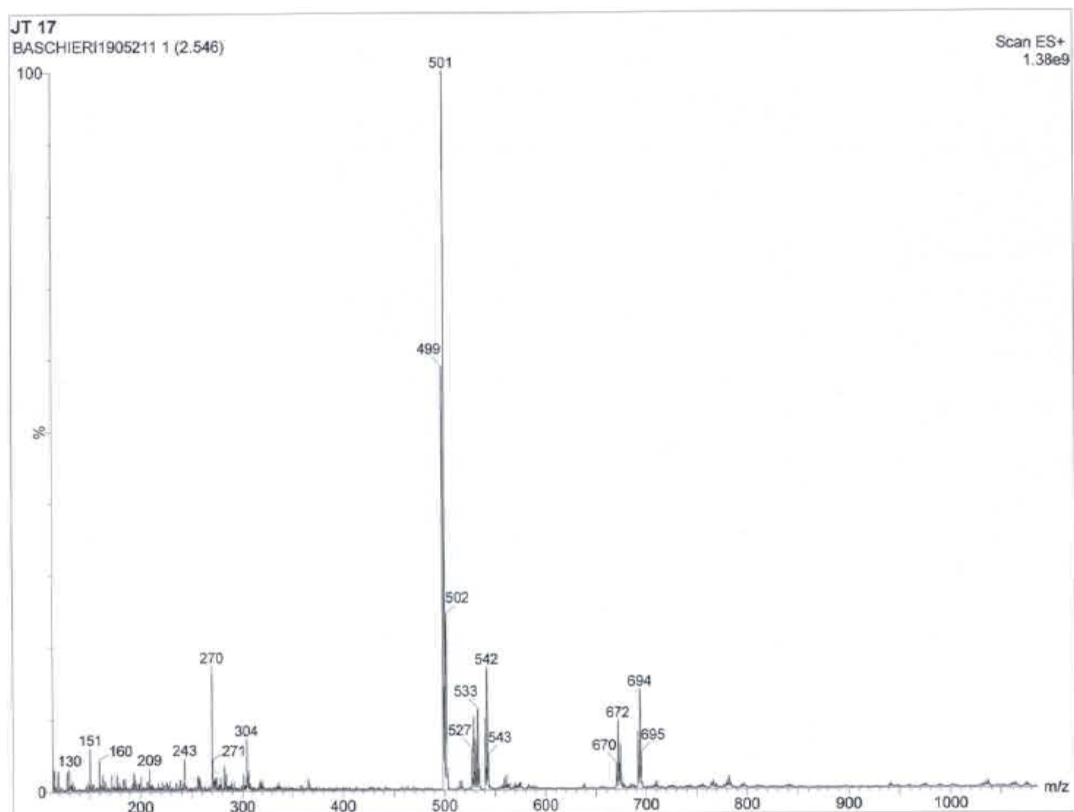


Fig. S15 ESI<sup>+</sup> spectrum of complex A.

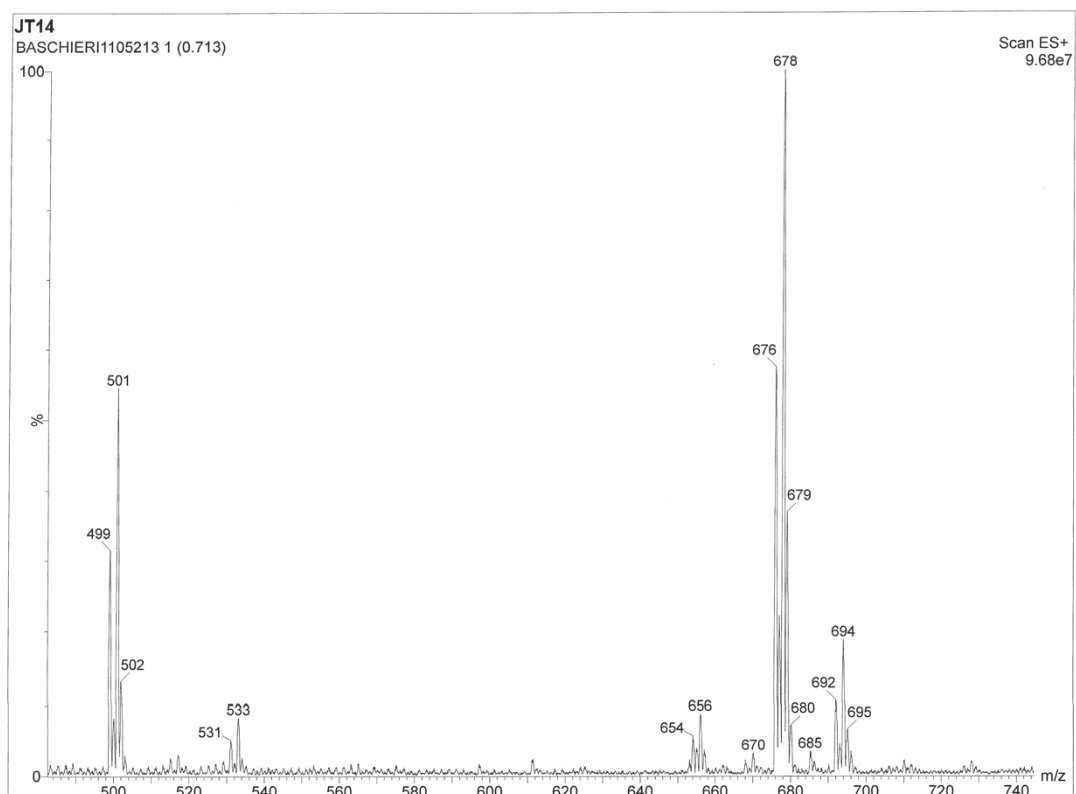
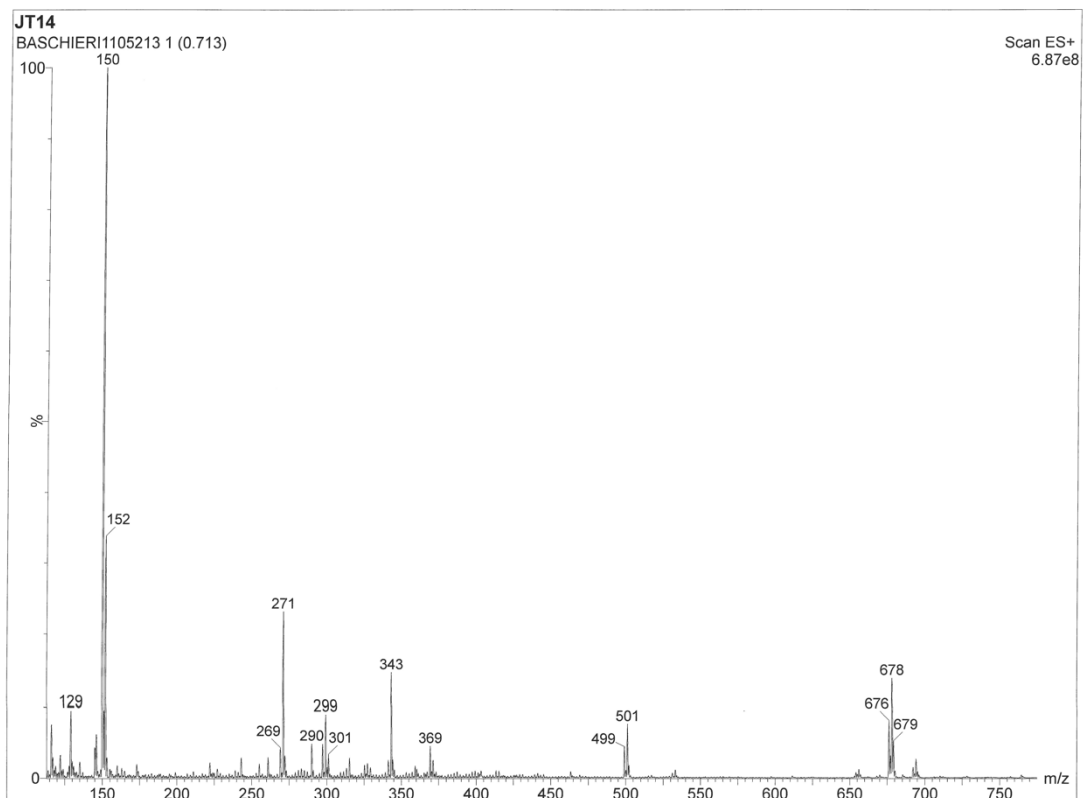
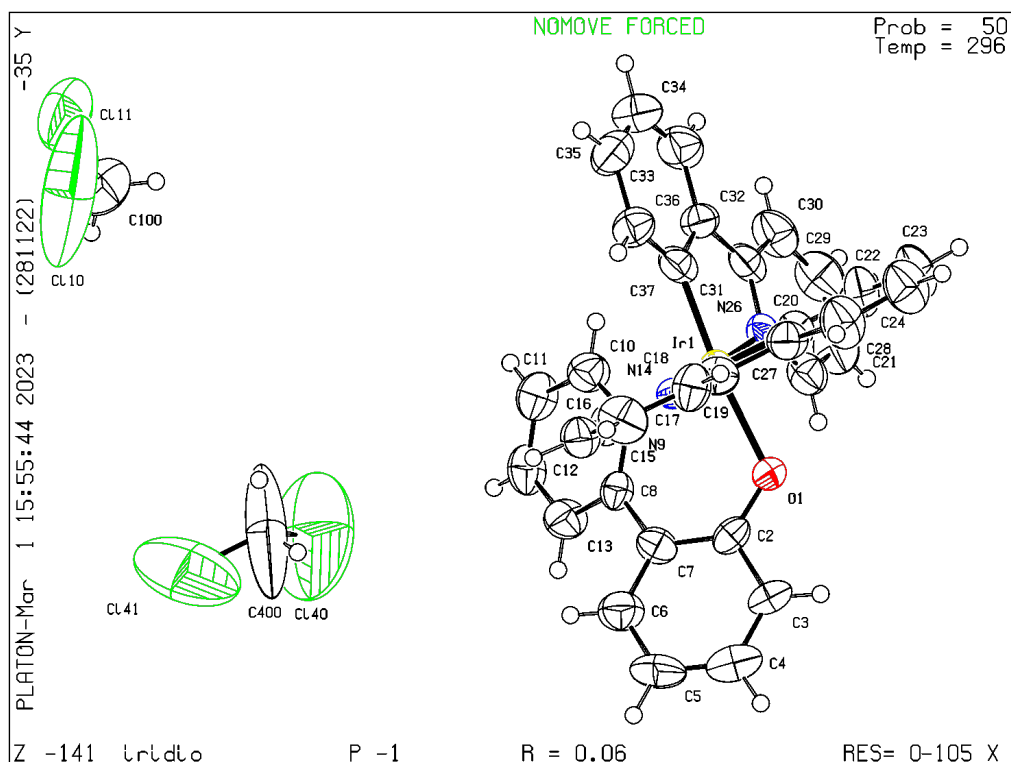


Fig. S16 ESI<sup>+</sup> spectrum of complex B.

## Crystal Structure Report for complex A



**Table S1** Sample and crystal data for complex A.

<b>Identification code</b>	leti1704	
<b>Chemical formula</b>	C <sub>35</sub> H <sub>28</sub> Cl <sub>4</sub> IrN <sub>3</sub> O	
<b>Formula weight</b>	840.60 g/mol	
<b>Temperature</b>	296(2) K	
<b>Wavelength</b>	0.71073 Å	
<b>Crystal size</b>	0.250 x 0.270 x 0.450 mm	
<b>Crystal system</b>	triclinic	
<b>Space group</b>	P-1	
<b>Unit cell dimensions</b>	a = 10.884(3) Å	α = 67.451(5) °
	b = 11.985(3) Å	β = 86.387(5) °
	c = 14.161(3) Å	γ = 79.182(5) °
<b>Volume</b>	1675.6(7) Å <sup>3</sup>	
<b>Z</b>	2	
<b>Density (calculated)</b>	1.666 g/cm <sup>3</sup>	
<b>Absorption coefficient</b>	4.336 mm <sup>-1</sup>	
<b>F(000)</b>	824	

**Table S2** Data collection and structure refinement for complex **A**.

<b>Theta range for data collection</b>	1.56 to 25.00°
<b>Index ranges</b>	-12<=h<=12, -14<=k<=14, -16<=l<=16
<b>Reflections collected</b>	18317
<b>Independent reflections</b>	5884 [R(int) = 0.1711]
<b>Coverage of independent reflections</b>	99.9%
<b>Absorption correction</b>	Multi-Scan
<b>Max. and min. transmission</b>	0.4100 and 0.2460
<b>Structure solution technique</b>	direct methods
<b>Structure solution program</b>	XT, VERSION 2014/5
<b>Refinement method</b>	Full-matrix least-squares on F <sup>2</sup>
<b>Refinement program</b>	SHELXL-2017/1 (Sheldrick, 2017)
<b>Function minimized</b>	$\sum w(F_o^2 - F_c^2)^2$
<b>Data / restraints / parameters</b>	5884 / 0 / 397
<b>Goodness-of-fit on F<sup>2</sup></b>	1.057
<b>Final R indices</b>	4652 data; $l > 2\sigma(l)$ R1 = 0.0593, wR2 = 0.1382 all data R1 = 0.0783, wR2 = 0.1475
<b>Weighting scheme</b>	$w = 1/[\sigma^2(F_o^2) + (0.0620P)^2]$ where $P = (F_o^2 + 2F_c^2)/3$
<b>Largest diff. peak and hole</b>	2.407 and -1.238 eÅ <sup>-3</sup>
<b>R.M.S. deviation from mean</b>	0.193 eÅ <sup>-3</sup>

**Table S3** Atomic coordinates and equivalent isotropic atomic displacement parameters (Å<sup>2</sup>) for complex **A**. U(eq) is defined as one third of the trace of the orthogonalized U<sub>ij</sub> tensor.

	x/a	y/b	z/c	U(eq)
Ir1	0.34095(3)	0.24579(3)	0.66540(2)	0.03900(15)
O1	0.2322(6)	0.1368(6)	0.6255(5)	0.0494(16)
N9	0.4683(8)	0.2135(7)	0.5507(6)	0.047(2)
N14	0.2402(7)	0.4086(6)	0.5702(5)	0.0397(17)
N26	0.4362(7)	0.0927(7)	0.7709(6)	0.0447(19)
C2	0.2145(9)	0.1553(7)	0.5290(7)	0.045(2)
C3	0.1013(10)	0.1316(8)	0.5037(9)	0.052(2)
C4	0.0731(12)	0.1530(11)	0.4041(11)	0.076(3)
C5	0.1564(13)	0.1979(11)	0.3245(10)	0.076(3)
C6	0.2691(12)	0.2167(10)	0.3501(9)	0.066(3)
C7	0.3018(9)	0.1905(8)	0.4505(7)	0.048(2)
C8	0.4349(9)	0.1859(7)	0.4734(7)	0.043(2)

C10	0.5920(10)	0.2091(10)	0.5637(8)	0.059(3)
C11	0.6859(10)	0.1755(11)	0.5048(9)	0.067(3)
C12	0.6545(11)	0.1421(10)	0.4298(9)	0.065(3)
C13	0.5286(10)	0.1475(9)	0.4113(8)	0.059(3)
C15	0.2647(10)	0.4714(8)	0.4721(8)	0.053(3)
C16	0.1988(11)	0.5815(9)	0.4133(8)	0.058(3)
C17	0.0968(13)	0.6324(9)	0.4553(9)	0.069(3)
C18	0.0691(10)	0.5699(8)	0.5567(8)	0.060(3)
C19	0.1370(10)	0.4593(8)	0.6128(8)	0.052(2)
C20	0.1214(10)	0.3840(10)	0.7213(8)	0.055(3)
C21	0.0185(11)	0.4133(11)	0.7782(9)	0.076(4)
C22	0.0127(12)	0.3400(12)	0.8813(10)	0.078(4)
C23	0.1005(13)	0.2419(12)	0.9258(9)	0.083(4)
C24	0.2033(10)	0.2089(9)	0.8680(7)	0.060(3)
C25	0.2125(10)	0.2807(8)	0.7617(7)	0.045(2)
C27	0.4189(11)	0.9773(8)	0.7901(8)	0.058(3)
C28	0.4866(13)	0.8771(9)	0.8603(9)	0.071(4)
C29	0.5806(13)	0.8915(10)	0.9157(9)	0.075(4)
C30	0.5996(11)	0.0074(10)	0.8976(8)	0.070(3)
C31	0.5251(10)	0.1084(10)	0.8240(7)	0.053(3)
C32	0.5351(10)	0.2392(9)	0.7997(8)	0.052(2)
C33	0.6141(12)	0.2772(12)	0.8489(9)	0.071(3)
C34	0.6157(14)	0.3997(13)	0.8224(11)	0.085(4)
C35	0.5378(12)	0.4860(11)	0.7441(10)	0.072(4)
C36	0.4547(11)	0.4478(9)	0.6953(8)	0.057(3)
C37	0.4508(10)	0.3215(10)	0.7208(7)	0.053(3)
Cl40	0.7508(14)	0.3687(8)	0.1403(11)	0.355(8)
Cl41	0.7429(10)	0.5766(7)	0.9586(6)	0.246(5)
C400	0.702(3)	0.5173(19)	0.076(2)	0.30(2)
Cl10	0.8970(7)	0.0900(7)	0.1337(9)	0.351(9)
Cl11	0.1166(5)	0.9467(6)	0.2373(5)	0.160(2)
C100	0.9741(18)	0.9454(19)	0.1959(15)	0.132(7)

**Table S4** Bond lengths (Å) for complex A.

Ir1-C37	1.984(11)	Ir1-C25	1.992(8)
Ir1-N26	2.013(8)	Ir1-N14	2.047(7)
Ir1-O1	2.158(7)	Ir1-N9	2.169(7)
O1-C2	1.318(11)	N9-C8	1.346(12)
N9-C10	1.359(14)	N14-C15	1.340(12)
N14-C19	1.392(11)	N26-C31	1.344(13)
N26-C27	1.350(11)	C2-C7	1.405(12)
C2-C3	1.412(14)	C3-C4	1.377(16)
C3-H3	0.93	C4-C5	1.404(17)
C4-H4	0.93	C5-C6	1.381(16)
C5-H5	0.93	C6-C7	1.388(14)
C6-H6	0.93	C7-C8	1.491(14)
C8-C13	1.431(12)	C10-C11	1.378(13)
C10-H10	0.93	C11-C12	1.352(16)
C11-H11	0.93	C12-C13	1.397(16)
C12-H12	0.93	C13-H13	0.93
C15-C16	1.351(14)	C15-H15	0.93
C16-C17	1.378(15)	C16-H16	0.93
C17-C18	1.385(14)	C17-H17	0.93
C18-C19	1.354(14)	C18-H18	0.93
C19-C20	1.472(14)	C20-C25	1.383(14)
C20-C21	1.408(13)	C21-C22	1.389(16)
C21-H21	0.93	C22-C23	1.334(18)
C22-H22	0.93	C23-C24	1.430(14)
C23-H23	0.93	C24-C25	1.426(13)
C24-H24	0.93	C27-C28	1.348(15)
C27-H27	0.93	C28-C29	1.402(18)
C28-H28	0.93	C29-C30	1.365(16)
C29-H29	0.93	C30-C31	1.406(14)
C30-H30	0.93	C31-C32	1.494(14)
C32-C33	1.379(15)	C32-C37	1.417(15)
C33-C34	1.372(16)	C33-H33	0.93
C34-C35	1.388(18)	C34-H34	0.93
C35-C36	1.408(16)	C35-H35	0.93
C36-C37	1.424(13)	C36-H36	0.93
Cl40-C400	1.66(2)	Cl41-C400	1.61(2)
C400-H40A	0.97	C400-H40B	0.97
Cl10-C100	1.69(2)	Cl11-C100	1.697(19)



C100-H10A

0.97

C100-H10B

0.97

**Table S5** Bond angles (°) for complex **A**.

C37-Ir1-C25	86.1(4)	C37-Ir1-N26	80.8(4)
C25-Ir1-N26	95.4(3)	C37-Ir1-N14	95.4(4)
C25-Ir1-N14	79.5(3)	N26-Ir1-N14	173.9(3)
C37-Ir1-O1	170.9(3)	C25-Ir1-O1	93.2(3)
N26-Ir1-O1	90.3(3)	N14-Ir1-O1	93.4(3)
C37-Ir1-N9	97.4(3)	C25-Ir1-N9	175.1(4)
N26-Ir1-N9	88.5(3)	N14-Ir1-N9	96.7(3)
O1-Ir1-N9	83.9(3)	C2-O1-Ir1	120.8(5)
C8-N9-C10	117.7(8)	C8-N9-Ir1	124.5(7)
C10-N9-Ir1	117.5(7)	C15-N14-C19	117.1(8)
C15-N14-Ir1	126.7(6)	C19-N14-Ir1	116.2(6)
C31-N26-C27	118.5(10)	C31-N26-Ir1	116.4(6)
C27-N26-Ir1	125.1(8)	O1-C2-C7	125.2(9)
O1-C2-C3	117.3(8)	C7-C2-C3	117.4(10)
C4-C3-C2	121.0(11)	C4-C3-H3	119.5
C2-C3-H3	119.5	C3-C4-C5	121.2(12)
C3-C4-H4	119.4	C5-C4-H4	119.4
C6-C5-C4	117.6(12)	C6-C5-H5	121.2
C4-C5-H5	121.2	C5-C6-C7	122.2(11)
C5-C6-H6	118.9	C7-C6-H6	118.9
C6-C7-C2	120.1(10)	C6-C7-C8	118.0(9)
C2-C7-C8	121.4(9)	N9-C8-C13	120.2(9)
N9-C8-C7	122.4(8)	C13-C8-C7	117.4(9)
N9-C10-C11	124.6(11)	N9-C10-H10	117.7
C11-C10-H10	117.7	C12-C11-C10	118.5(11)
C12-C11-H11	120.8	C10-C11-H11	120.8
C11-C12-C13	119.6(9)	C11-C12-H12	120.2
C13-C12-H12	120.2	C12-C13-C8	119.4(10)
C12-C13-H13	120.3	C8-C13-H13	120.3
N14-C15-C16	124.6(9)	N14-C15-H15	117.7
C16-C15-H15	117.7	C15-C16-C17	118.5(10)
C15-C16-H16	120.8	C17-C16-H16	120.8
C16-C17-C18	118.4(10)	C16-C17-H17	120.8
C18-C17-H17	120.8	C19-C18-C17	121.3(10)

C19-C18-H18	119.3	C17-C18-H18	119.3
C18-C19-N14	120.0(9)	C18-C19-C20	127.6(9)
N14-C19-C20	112.2(8)	C25-C20-C21	122.8(10)
C25-C20-C19	115.1(8)	C21-C20-C19	122.1(10)
C22-C21-C20	118.6(12)	C22-C21-H21	120.7
C20-C21-H21	120.7	C23-C22-C21	121.3(11)
C23-C22-H22	119.3	C21-C22-H22	119.3
C22-C23-C24	120.5(11)	C22-C23-H23	119.7
C24-C23-H23	119.7	C25-C24-C23	120.1(10)
C25-C24-H24	119.9	C23-C24-H24	119.9
C20-C25-C24	116.4(8)	C20-C25-Ir1	116.8(7)
C24-C25-Ir1	126.8(7)	C28-C27-N26	123.0(12)
C28-C27-H27	118.5	N26-C27-H27	118.5
C27-C28-C29	119.3(11)	C27-C28-H28	120.4
C29-C28-H28	120.4	C30-C29-C28	118.7(11)
C30-C29-H29	120.7	C28-C29-H29	120.7
C29-C30-C31	119.4(12)	C29-C30-H30	120.3
C31-C30-H30	120.3	N26-C31-C30	121.1(11)
N26-C31-C32	114.7(9)	C30-C31-C32	124.2(11)
C33-C32-C37	123.2(10)	C33-C32-C31	124.7(11)
C37-C32-C31	112.0(10)	C34-C33-C32	120.8(13)
C34-C33-H33	119.6	C32-C33-H33	119.6
C33-C34-C35	119.4(13)	C33-C34-H34	120.3
C35-C34-H34	120.3	C34-C35-C36	120.0(11)
C34-C35-H35	120.0	C36-C35-H35	120.0
C35-C36-C37	122.0(11)	C35-C36-H36	119.0
C37-C36-H36	119.0	C32-C37-C36	114.5(10)
C32-C37-Ir1	116.0(8)	C36-C37-Ir1	129.4(9)
Cl41-C400-Cl40	118.5(14)	Cl41-C400-H40A	107.7
Cl40-C400-H40A	107.7	Cl41-C400-H40B	107.7
Cl40-C400-H40B	107.7	H40A-C400-H40B	107.1
Cl10-C100-Cl11	110.9(11)	Cl10-C100-H10A	109.5
Cl11-C100-H10A	109.5	Cl10-C100-H10B	109.5
Cl11-C100-H10B	109.5	H10A-C100-H10B	108.1

**Table S6.** Torsional angles (°) for complex **A**.

Ir1-O1-C2-C7	34.4(11)	Ir1-O1-C2-C3	-149.0(6)
O1-C2-C3-C4	177.5(9)	C7-C2-C3-C4	-5.7(13)
C2-C3-C4-C5	0.6(16)	C3-C4-C5-C6	1.7(18)
C4-C5-C6-C7	1.2(18)	C5-C6-C7-C2	-6.5(16)
C5-C6-C7-C8	166.1(10)	O1-C2-C7-C6	-174.9(9)
C3-C2-C7-C6	8.5(13)	O1-C2-C7-C8	12.8(13)
C3-C2-C7-C8	-163.8(8)	C10-N9-C8-C13	3.1(13)
Ir1-N9-C8-C13	-170.2(6)	C10-N9-C8-C7	-178.6(9)
Ir1-N9-C8-C7	8.2(12)	C6-C7-C8-N9	151.0(9)
C2-C7-C8-N9	-36.6(13)	C6-C7-C8-C13	-30.6(13)
C2-C7-C8-C13	141.9(9)	C8-N9-C10-C11	-1.7(16)
Ir1-N9-C10-C11	172.1(9)	N9-C10-C11-C12	-1.2(18)
C10-C11-C12-C13	2.6(18)	C11-C12-C13-C8	-1.2(17)
N9-C8-C13-C12	-1.7(14)	C7-C8-C13-C12	179.8(10)
C19-N14-C15-C16	2.3(16)	Ir1-N14-C15-C16	-176.8(8)
N14-C15-C16-C17	-2.0(18)	C15-C16-C17-C18	2.0(18)
C16-C17-C18-C19	-2.6(19)	C17-C18-C19-N14	2.9(17)
C17-C18-C19-C20	178.1(11)	C15-N14-C19-C18	-2.6(15)
Ir1-N14-C19-C18	176.6(8)	C15-N14-C19-C20	-178.5(9)
Ir1-N14-C19-C20	0.7(11)	C18-C19-C20-C25	-173.5(11)
N14-C19-C20-C25	2.1(13)	C18-C19-C20-C21	8.7(19)
N14-C19-C20-C21	-175.7(10)	C25-C20-C21-C22	4.5(19)
C19-C20-C21-C22	-177.8(11)	C20-C21-C22-C23	-2.(2)
C21-C22-C23-C24	0.(2)	C22-C23-C24-C25	0.(2)
C21-C20-C25-C24	-5.0(17)	C19-C20-C25-C24	177.2(10)
C21-C20-C25-Ir1	173.9(9)	C19-C20-C25-Ir1	-3.9(12)
C23-C24-C25-C20	2.8(16)	C23-C24-C25-Ir1	-175.9(10)
C31-N26-C27-C28	0.0(14)	Ir1-N26-C27-C28	178.7(8)
N26-C27-C28-C29	-0.7(16)	C27-C28-C29-C30	0.9(18)
C28-C29-C30-C31	-0.3(17)	C27-N26-C31-C30	0.6(12)
Ir1-N26-C31-C30	-178.3(7)	C27-N26-C31-C32	-178.3(7)
Ir1-N26-C31-C32	2.8(9)	C29-C30-C31-N26	-0.4(15)
C29-C30-C31-C32	178.4(9)	N26-C31-C32-C33	175.9(9)
C30-C31-C32-C33	-2.9(15)	N26-C31-C32-C37	-2.6(11)
C30-C31-C32-C37	178.6(8)	C37-C32-C33-C34	-0.7(17)
C31-C32-C33-C34	-179.0(10)	C32-C33-C34-C35	-0.8(19)
C33-C34-C35-C36	2.4(18)	C34-C35-C36-C37	-2.6(16)
C33-C32-C37-C36	0.6(14)	C31-C32-C37-C36	179.1(8)
C33-C32-C37-Ir1	-177.4(8)	C31-C32-C37-Ir1	1.2(10)

C35-C36-C37-C32

1.1(14)

C35-C36-C37-Ir1

178.7(7)

**Table S7** Anisotropic atomic displacement parameters ( $\text{\AA}^2$ ) for complex **A**. The anisotropic atomic displacement factor exponent takes the form:  $-2\pi^2 [h^2 a^{*2} U_{11} + \dots + 2 h k a^* b^* U_{12}]$ .

	U11	U22	U33	U23	U13	U12
Ir1	0.0353(2)	0.0410(2)	0.0392(2)	-0.01418(15)	0.00110(16)	-0.00562(16)
O1	0.053(4)	0.058(4)	0.040(4)	-0.015(3)	-0.001(3)	-0.026(3)
N9	0.047(5)	0.043(4)	0.050(5)	-0.020(4)	0.005(4)	-0.005(4)
N14	0.038(4)	0.047(4)	0.037(4)	-0.015(3)	-0.004(3)	-0.012(3)
N26	0.039(4)	0.056(4)	0.040(4)	-0.020(4)	0.009(4)	-0.009(4)
C2	0.043(5)	0.031(4)	0.061(6)	-0.017(4)	-0.002(5)	-0.009(4)
C3	0.046(6)	0.046(5)	0.070(7)	-0.027(5)	-0.012(5)	-0.011(5)
C4	0.071(8)	0.076(8)	0.097(10)	-0.047(8)	-0.023(8)	-0.011(7)
C5	0.084(10)	0.085(8)	0.065(8)	-0.035(7)	-0.033(7)	-0.005(7)
C6	0.068(8)	0.072(7)	0.063(7)	-0.027(6)	-0.009(6)	-0.015(6)
C7	0.049(6)	0.050(5)	0.044(5)	-0.018(4)	-0.006(5)	0.000(5)
C8	0.042(5)	0.036(4)	0.048(5)	-0.014(4)	0.006(4)	-0.008(4)
C10	0.050(6)	0.071(6)	0.060(6)	-0.029(5)	-0.001(5)	-0.011(6)
C11	0.032(5)	0.090(8)	0.081(8)	-0.037(7)	0.013(6)	-0.008(6)
C12	0.048(7)	0.074(7)	0.071(8)	-0.031(6)	0.023(6)	-0.007(6)
C13	0.057(7)	0.065(6)	0.066(7)	-0.040(5)	0.009(6)	-0.008(5)
C15	0.047(6)	0.051(5)	0.057(6)	-0.017(5)	0.008(5)	-0.012(5)
C16	0.068(7)	0.053(5)	0.050(6)	-0.014(5)	-0.001(6)	-0.015(6)
C17	0.088(9)	0.039(5)	0.068(7)	-0.014(5)	-0.011(7)	0.007(6)
C18	0.058(7)	0.044(5)	0.069(7)	-0.014(5)	0.007(6)	-0.008(5)
C19	0.057(6)	0.044(5)	0.057(6)	-0.022(4)	-0.006(5)	-0.002(5)
C20	0.043(6)	0.070(6)	0.061(6)	-0.035(5)	0.005(5)	-0.010(5)
C21	0.054(7)	0.091(8)	0.078(8)	-0.033(7)	0.014(7)	-0.001(7)
C22	0.050(7)	0.101(9)	0.072(8)	-0.031(7)	0.011(7)	0.005(7)
C23	0.084(10)	0.102(9)	0.052(7)	-0.023(7)	0.023(7)	-0.014(8)
C24	0.053(6)	0.062(6)	0.048(6)	-0.006(5)	0.012(5)	-0.003(5)
C25	0.046(6)	0.046(5)	0.043(5)	-0.017(4)	0.001(5)	-0.007(5)
C27	0.077(8)	0.046(5)	0.050(6)	-0.017(4)	0.005(6)	-0.010(5)
C28	0.082(9)	0.047(6)	0.072(8)	-0.016(5)	0.003(7)	0.002(6)
C29	0.084(9)	0.057(6)	0.062(7)	-0.008(6)	-0.013(7)	0.009(7)
C30	0.059(7)	0.082(8)	0.050(6)	-0.011(6)	-0.012(6)	0.006(6)
C31	0.046(6)	0.076(6)	0.034(5)	-0.020(5)	0.003(5)	-0.005(5)
C32	0.049(6)	0.062(6)	0.055(6)	-0.032(5)	0.005(5)	-0.018(5)

C33	0.057(7)	0.091(8)	0.061(7)	-0.025(7)	-0.009(6)	-0.010(7)
C34	0.091(11)	0.105(10)	0.083(10)	-0.051(9)	-0.001(8)	-0.040(9)
C35	0.064(8)	0.079(8)	0.095(10)	-0.050(8)	0.021(7)	-0.031(7)
C36	0.063(7)	0.046(5)	0.065(7)	-0.023(5)	-0.001(6)	-0.012(5)
C37	0.044(6)	0.075(6)	0.040(5)	-0.026(5)	0.002(5)	-0.006(5)
Cl40	0.437(19)	0.142(6)	0.442(17)	-0.077(9)	0.158(15)	-0.070(10)
Cl41	0.369(14)	0.191(6)	0.206(7)	-0.139(6)	-0.063(8)	0.046(8)
C400	0.39(5)	0.105(15)	0.31(4)	-0.023(19)	0.28(4)	-0.05(2)
Cl10	0.119(5)	0.195(7)	0.463(16)	0.152(8)	0.074(8)	0.008(5)
Cl11	0.112(4)	0.191(5)	0.180(5)	-0.059(5)	0.037(4)	-0.071(4)
C100	0.110(14)	0.168(18)	0.131(15)	-0.051(14)	0.002(12)	-0.065(14)

**Table S8** Hydrogen atomic coordinates and isotropic atomic displacement parameters ( $\text{\AA}^2$ ) for **A**.

	x/a	y/b	z/c	U(eq)
H3	0.0448	0.1010	0.5551	0.062
H4	-0.0025	0.1374	0.3892	0.091
H5	0.1365	0.2144	0.2570	0.091
H6	0.3249	0.2479	0.2983	0.08
H10	0.6148	0.2304	0.6159	0.07
H11	0.7690	0.1757	0.5164	0.081
H12	0.7164	0.1158	0.3908	0.078
H13	0.5058	0.1262	0.3590	0.07
H15	0.3317	0.4367	0.4423	0.064
H16	0.2218	0.6220	0.3462	0.07
H17	0.0477	0.7068	0.4165	0.083
H18	0.0025	0.6047	0.5868	0.072
H21	-0.0443	0.4804	0.7475	0.092
H22	-0.0537	0.3598	0.9200	0.094
H23	0.0948	0.1945	0.9950	0.099
H24	0.2642	0.1404	0.8997	0.072
H27	0.3574	-0.0335	0.7533	0.07
H28	0.4711	-0.2008	0.8718	0.085
H29	0.6292	-0.1764	0.9637	0.09
H30	0.6611	0.0194	0.9336	0.084
H33	0.6670	0.2191	0.9007	0.085
H34	0.6685	0.4247	0.8565	0.102
H35	0.5406	0.5690	0.7239	0.087

H36	0.4008	0.5069	0.6448	0.068
H40A	0.6113	0.5326	0.0777	0.358
H40B	0.7309	0.5614	0.1125	0.358
H10A	0.9843	0.9011	0.1504	0.159
H10B	0.9253	0.9031	0.2540	0.159

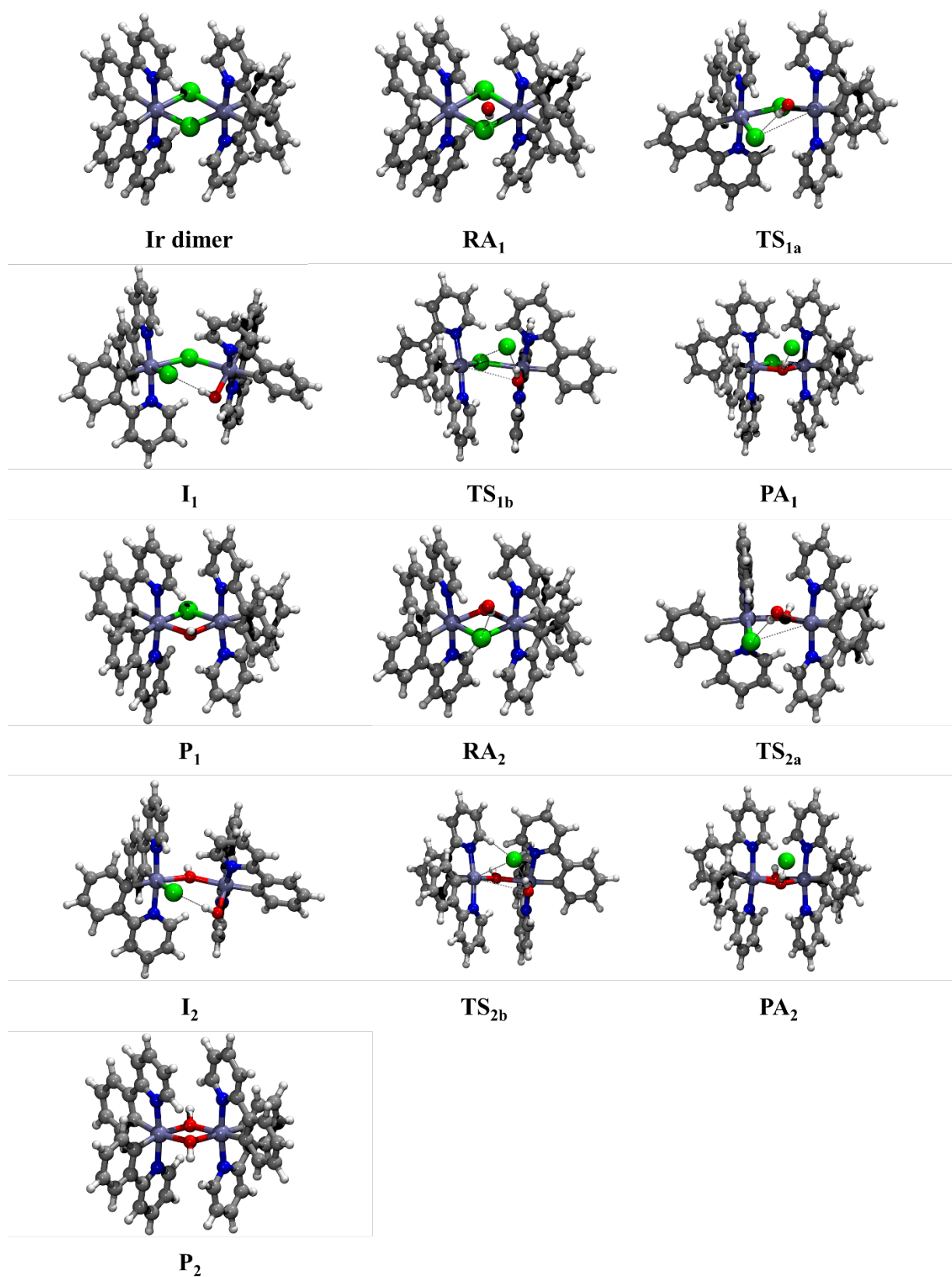
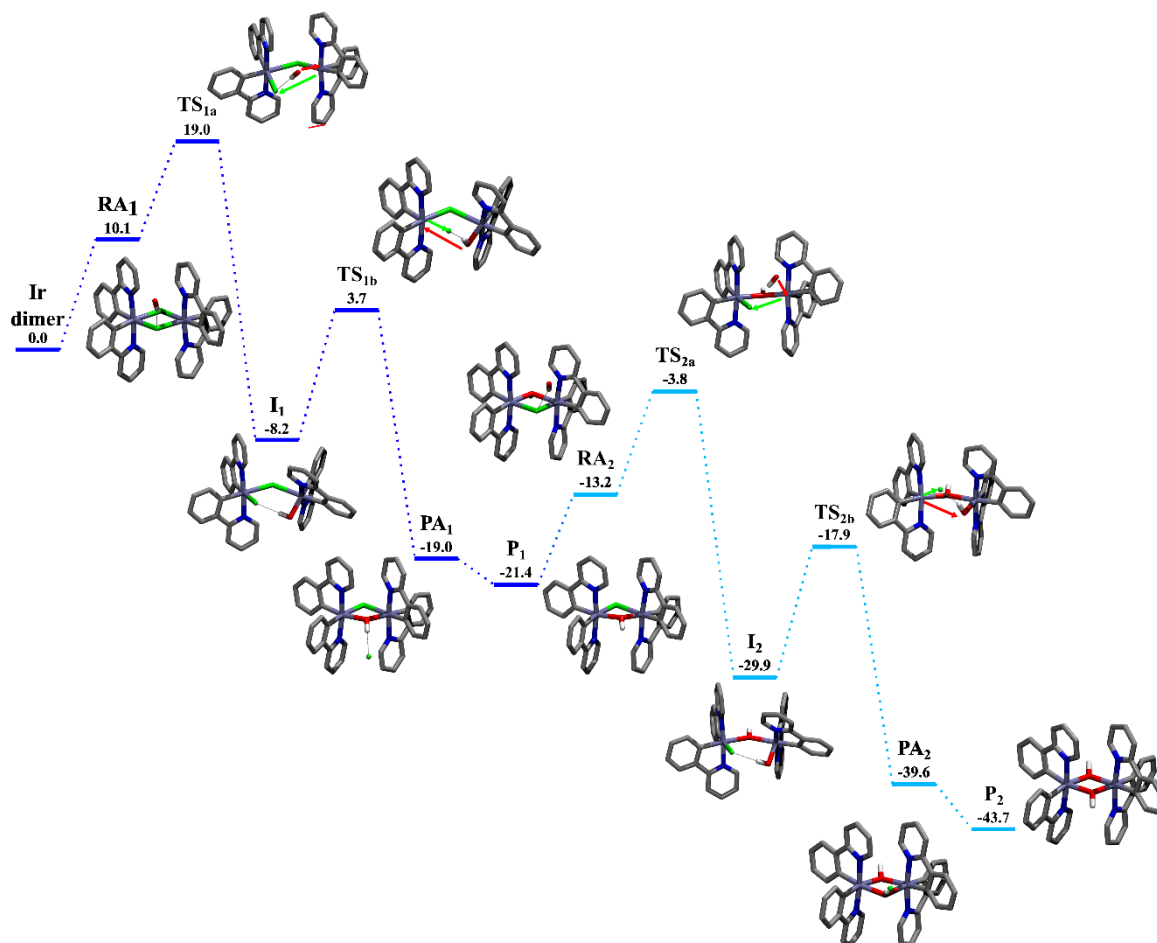


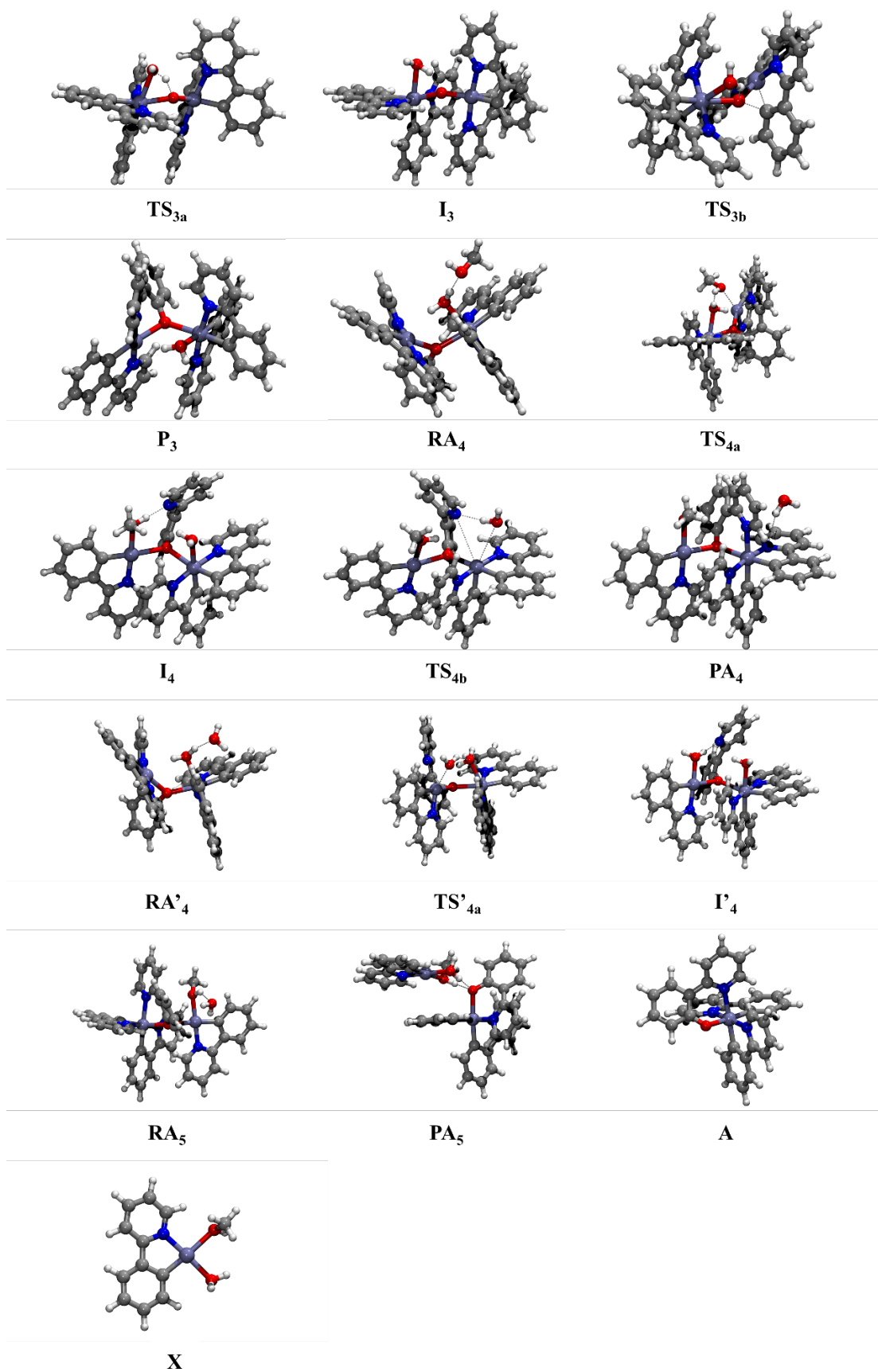
**Fig. S17** Optimized structures for the first and second hydrolysis stages of  $[\text{Ir}(\text{ppy})_2\text{Cl}]_2$ .



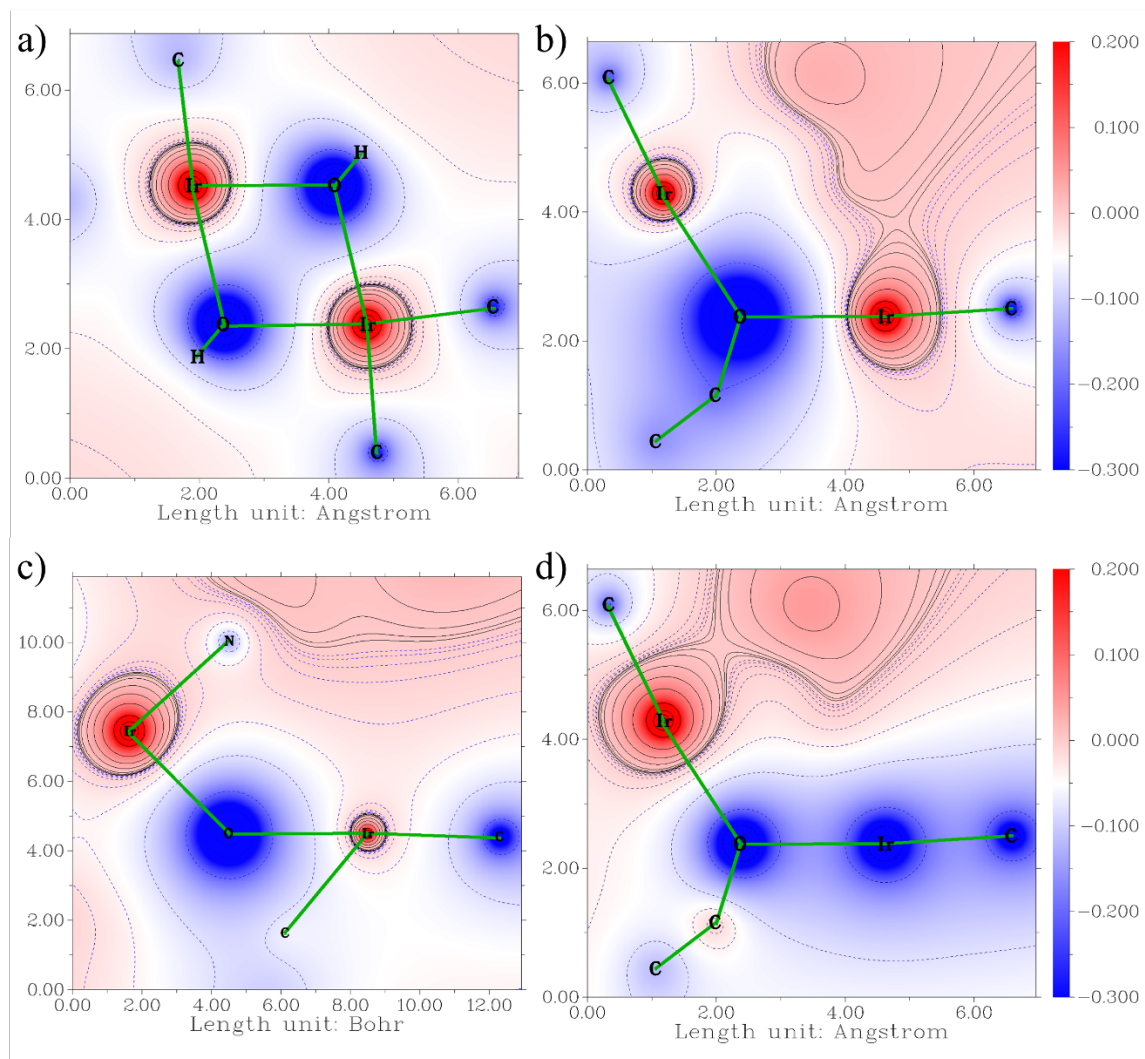
— first hydrolysis — STEP-I — second hydrolysis —

**Fig. S18** Calculated free energy profile in methanol for the two-hydrolysis stages (first hydrolysis in blue, second in light blue) of  $[\text{Ir}(\text{ppy})_2\text{Cl}]_2$ . Gibbs free energies (reported below the label name of complex) are in  $\text{kcal}\cdot\text{mol}^{-1}$  and are related to separated reactants (**Ir-dimer** is 0.0 by definition).





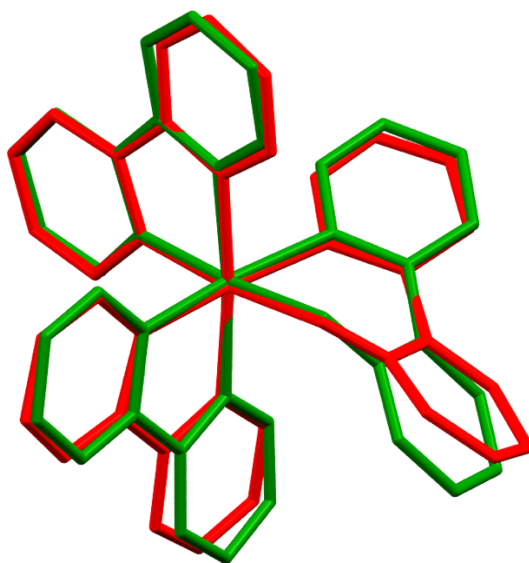
**Fig. S19** Optimized structures for steps II to IV of the proposed reaction mechanism.



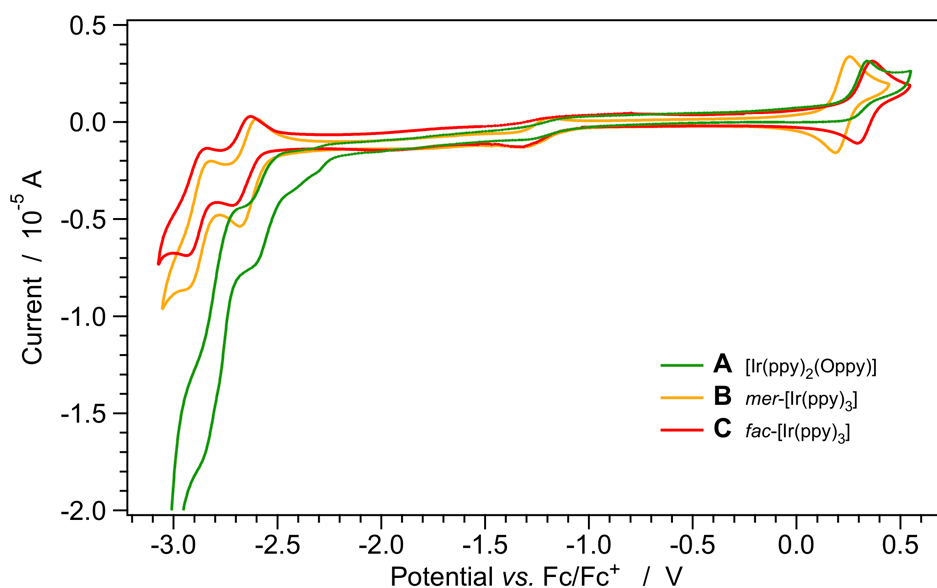
**Fig. S20** 2D plot related to electrostatic potential from Hirshfeld charges along the Ir–O–Ir plane for: a)  $P_2$ ; b)  $I_3$ ; c)  $TS_{3b}$ ; d)  $P_3$ . In  $P_2$  and  $I_3$  complexes, the two iridium atoms show similar positive Hirshfeld charge values, while in  $P_3$  the octahedral iridium(III) moieties keep the positive charge value and the square-planar iridium(I) site show a negative Hirshfeld charge, indicating the change of the oxidation state.

**Table S9** Relative Gibbs free energy values (kcal mol<sup>-1</sup>) associated to the overall reaction pathway (including all four steps)

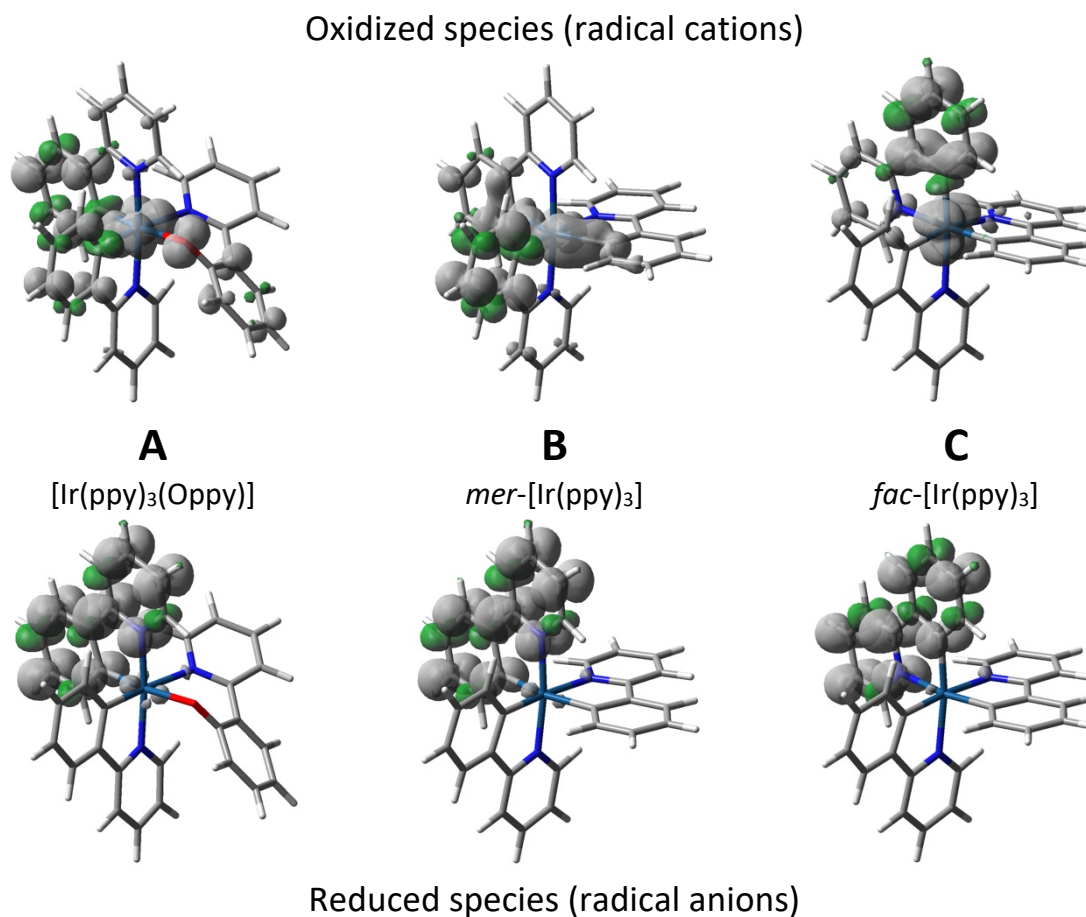
<i>I step – hydrolysis reaction</i>					
<b>Ir dimer → RA<sub>1</sub></b>	<b>RA<sub>1</sub> → TS<sub>1a</sub></b>	<b>TS<sub>1a</sub> → I<sub>1</sub></b>	<b>I<sub>1</sub> → TS<sub>1b</sub></b>	<b>TS<sub>1b</sub> → PA<sub>1</sub></b>	<b>PA<sub>1</sub> → P<sub>1</sub></b>
10.1	8.9	-27.2	11.9	-22.7	-2.4
<b>P<sub>1</sub> → RA<sub>2</sub></b>	<b>RA<sub>2</sub> → TS<sub>2a</sub></b>	<b>TS<sub>2b</sub> → I<sub>2</sub></b>	<b>I<sub>2</sub> → TS<sub>2b</sub></b>	<b>TS<sub>2b</sub> → PA<sub>2</sub></b>	<b>PA<sub>2</sub> → P<sub>2</sub></b>
8.2	9.4	-26.1	12.0	-21.7	-4.1
<i>II Step – C-O Formation</i>					
<b>P<sub>2</sub> → TS<sub>3a</sub></b>	<b>TS<sub>3a</sub> → I<sub>3</sub></b>	<b>I<sub>3b</sub> → TS<sub>3b</sub></b>	<b>TS<sub>3b</sub> → P<sub>3</sub></b>		
22.6	0.4	35.1	-31.9		
<i>III Step – Ir-N Formation</i>					
<b>P<sub>3</sub> → RA<sub>4</sub></b>	<b>RA<sub>4</sub> → TS<sub>4a</sub></b>	<b>TS<sub>4a</sub> → I<sub>4</sub></b>	<b>I<sub>4</sub> → TS<sub>4b</sub></b>	<b>TS<sub>4b</sub> → PA<sub>4</sub></b>	
2.3	36.9	-12.7	9.0	-20.4	
<b>P<sub>3</sub> → RA'<sub>4</sub></b>	<b>RA<sub>4</sub> → TS'<sub>4a</sub></b>	<b>TS'<sub>4a</sub> → I<sub>4</sub></b>			
1.7	39.3	-14.9			
<i>IV – Final product</i>					
<b>PA<sub>4</sub> → RA<sub>5</sub></b>	<b>RA<sub>5</sub> → TS<sub>5</sub></b>	<b>TS<sub>5</sub> → PA<sub>5</sub></b>	<b>PA<sub>5</sub> → A + X</b>		
-5.3	11.2	-9.4	9.2		



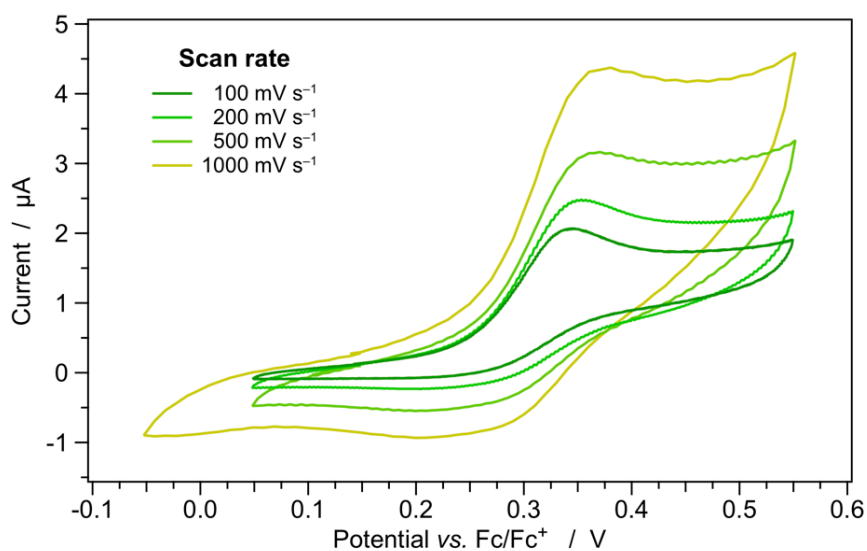
**Fig. S21** Structural overlap (H atoms omitted for clarity) between the experimental X-ray structure of complex **A** (red) and the DFT-computed one (green). The overlap is calculated by minimizing the root-mean-square deviation (RMSD) of all the atomic positions; RMSD = 0.350 Å.



**Fig. S22** Cyclic voltammograms of complexes **A–C** (0.5 mM) in acetonitrile solution at 298 K, recorded at a scan rate of 100 mV s<sup>-1</sup>. The voltammograms show the full reversibility of all redox process of the two [Ir(ppy)<sub>3</sub>] isomers (**B** and **C**); on the contrary, irreversibility is observed for the oxidation process of novel [Ir(ppy)<sub>2</sub>(Oppy)] complex (**A**).

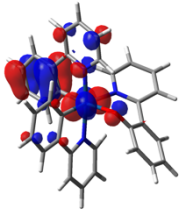
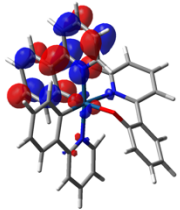
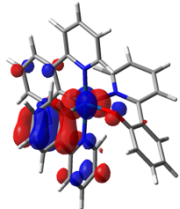
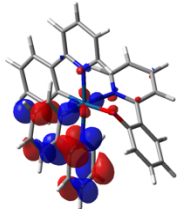
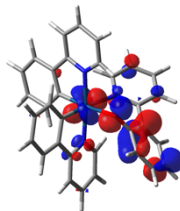
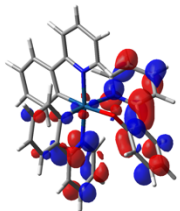
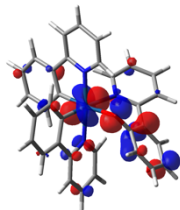
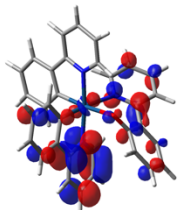
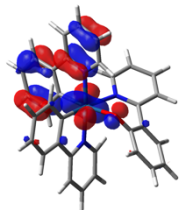
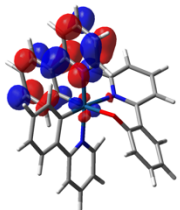
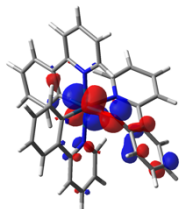
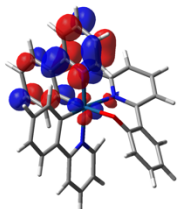


**Fig. S23** Spin-density distribution of the oxidized and reduced radicals of **A–C** in their fully-relaxed geometry, computed by spin-unrestricted DFT in acetonitrile (isovalues: 0.002 e bohr<sup>-3</sup>).

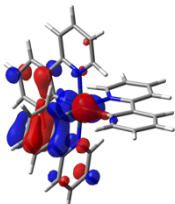
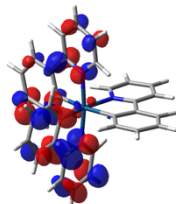
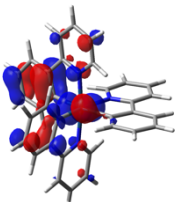
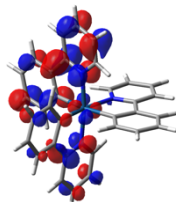
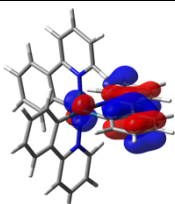
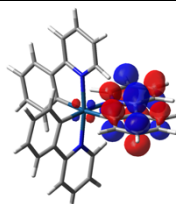
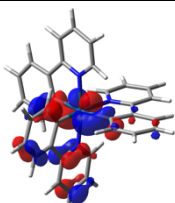
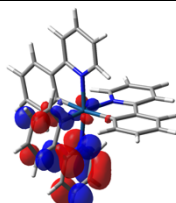
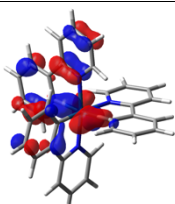
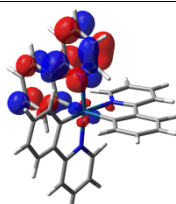
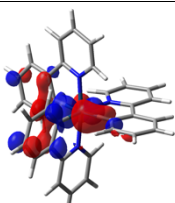
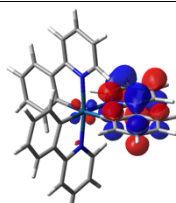


**Fig. S24** Anodic cyclic voltammograms of complex [Ir(ppy)<sub>2</sub>(Oppy)] (**A**) at different scan rates in acetonitrile solution at 298 K (sample concentration: 0.5 mM). Experiments show the complete irreversibility of the oxidation process.

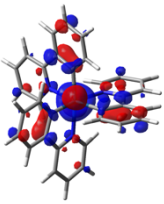
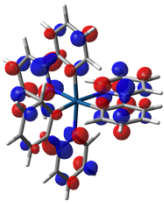
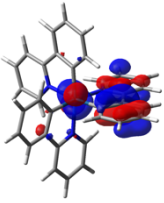
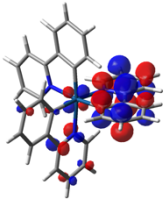
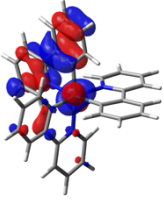
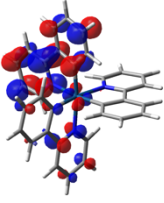
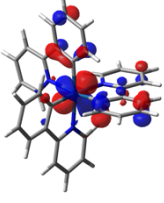
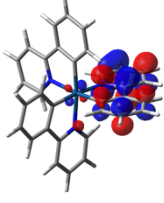
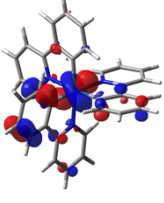
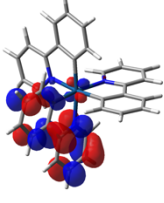
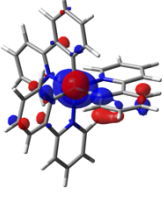
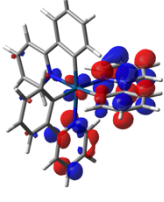
**Table S10** Calculated NTOs couples describing the lowest six triplet excitations for [Ir(ppy)<sub>2</sub>(Oppy)] (**A**) in acetonitrile. The  $\lambda$  value is the natural transition orbital eigenvalue associated with each NTOs couple; orbital isovalue:  $0.04 e^{-1/2} \text{ bohr}^{-3/2}$ .

	Transition energy [eV (nm)]	NTO couple hole $\rightarrow$ electron ( $\lambda$ )		Nature
$S_0 \rightarrow T_1$	2.58 (481)			mainly <sup>3</sup> LC on the ppy <sub>a</sub> ligand with minor <sup>3</sup> MLCT contribution
		(93.1%)		
$S_0 \rightarrow T_2$	2.64 (469)			mainly <sup>3</sup> LC on the ppy <sub>b</sub> ligand with minor <sup>3</sup> MLCT contribution
		(88.0%)		
$S_0 \rightarrow T_3$	2.76 (449)			mainly <sup>3</sup> LC on the Oppy ligand with minor <sup>3</sup> MLCT contribution
		(75.0%)		
$S_0 \rightarrow T_4$	2.85 (435)			mixed <sup>3</sup> LC/ <sup>3</sup> LL'CT involving the Oppy and ppy <sub>b</sub> ligands with minor <sup>3</sup> MLCT contribution
		(75.4%)		
$S_0 \rightarrow T_5$	3.01 (412)			mainly <sup>3</sup> LC on the ppy <sub>a</sub> ligand with minor <sup>3</sup> MLCT contribution
		(75.1%)		
$S_0 \rightarrow T_6$	3.19 (388)			mainly <sup>3</sup> MLCT from iridium to the ppy <sub>a</sub> ligand with minor <sup>3</sup> LL'CT contribution involving Oppy
		(92.7%)		

**Table S11** Calculated NTOs couples describing the lowest six triplet excitations for *mer*-Ir(ppy)<sub>3</sub> (**B**) in acetonitrile. The  $\lambda$  value is the natural transition orbital eigenvalue associated with each NTOs couple; orbital isovalue:  $0.04 e^{-1/2} \text{ bohr}^{-3/2}$ .

	Transition energy [eV (nm)]	NTO couple hole $\rightarrow$ electron ( $\lambda$ )		Nature
$S_0 \rightarrow T_1$	2.64 (470)			mainly <sup>3</sup> LC on the <i>trans</i> -ppy ligands with minor <sup>3</sup> MLCT contribution
		(82.9%)		
$S_0 \rightarrow T_2$	2.69 (461)			mainly <sup>3</sup> LC on the <i>trans</i> -ppy ligands with minor <sup>3</sup> MLCT contribution
		(75.6%)		
$S_0 \rightarrow T_3$	2.79 (444)			mainly <sup>3</sup> LC on the <i>equatorial</i> -ppy ligand with minor <sup>3</sup> MLCT contribution
		(90.8%)		
$S_0 \rightarrow T_4$	2.88 (431)			mainly <sup>3</sup> LC on the <i>trans</i> -ppy ligands with minor <sup>3</sup> MLCT contribution
		(87.0%)		
$S_0 \rightarrow T_5$	2.96 (418)			mainly <sup>3</sup> LC on the <i>trans</i> -ppy ligands with minor <sup>3</sup> MLCT contribution
		(80.6%)		
$S_0 \rightarrow T_6$	3.05 (407)			mainly <sup>3</sup> MLCT from iridium to <i>equatorial</i> -ppy ligand
		(96.3%)		

**Table S12** Calculated NTOs couples describing the lowest six triplet excitations for *fac*-Ir(ppy)<sub>3</sub> (**C**) in acetonitrile. The  $\lambda$  value is the natural transition orbital eigenvalue associated with each NTOs couple; orbital isovalue:  $0.04 e^{-1/2} \text{ bohr}^{-3/2}$ .

	Transition energy [eV (nm)]	NTO couple hole $\rightarrow$ electron ( $\lambda$ )		Nature
$S_0 \rightarrow T_1$	2.72 (456)			mainly <sup>3</sup> MLTC from iridium to ppy ligands with minor <sup>3</sup> LC contribution
		(65.7%)		
$S_0 \rightarrow T_2$	2.76 (449)			mainly <sup>3</sup> MLTC from iridium to a ppy ligand with <sup>3</sup> LC contribution
		(63.5%)		
$S_0 \rightarrow T_3$	2.77 (447)			mainly <sup>3</sup> MLTC from iridium to a ppy ligand with <sup>3</sup> LC contribution
		(59.3%)		
$S_0 \rightarrow T_4$	3.15 (393)			mainly <sup>3</sup> MLTC from iridium to a ppy ligand with minor <sup>3</sup> LC contribution
		(88.9%)		
$S_0 \rightarrow T_5$	3.20 (388)			mainly <sup>3</sup> MLTC from iridium to a ppy ligand with minor <sup>3</sup> LC contribution
		(82.3%)		
$S_0 \rightarrow T_6$	3.22 (385)			mainly <sup>3</sup> MLTC from iridium to a ppy ligand with minor <sup>3</sup> LC contribution
		(56.1%)		



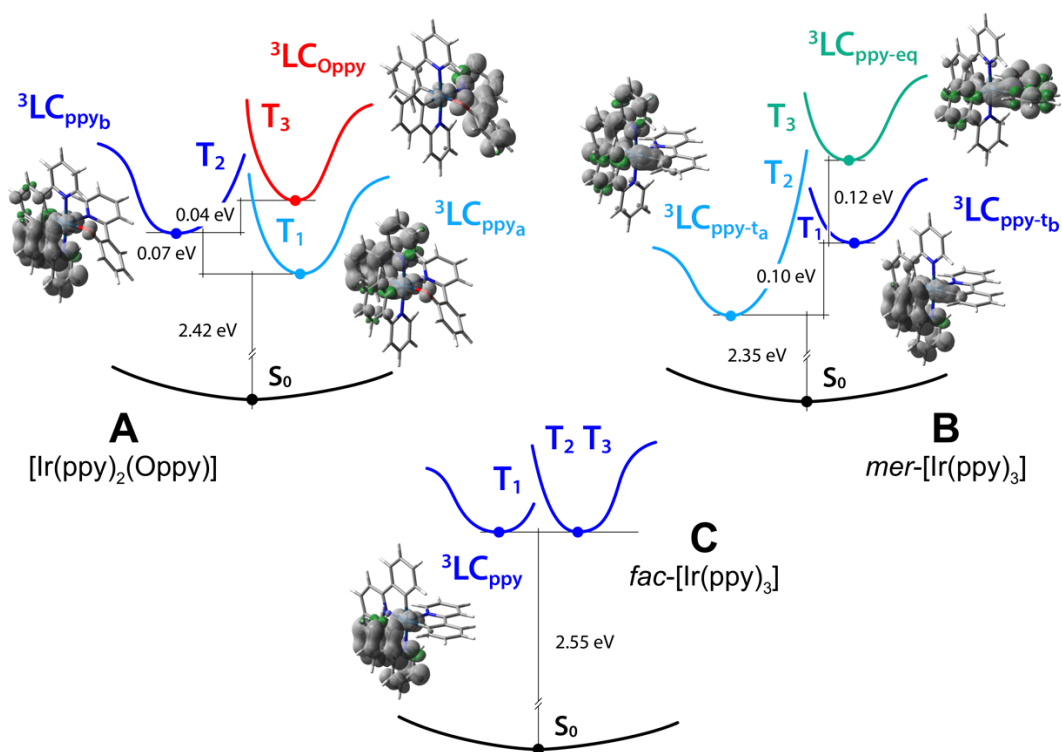


**Fig. S25** Schematic energy diagram reporting the ground state ( $S_0$ ) and the three lowest triplet states ( $T_1$ ,  $T_2$  and  $T_3$ , numbered following the order of Tables S10–12) of complexes **A–C**. The spin-density surfaces, calculated at the fully-relaxed triplet-state minima, are also depicted (isovalue:  $0.002 \text{ e bohr}^{-3}$ ). Reported energy values refer to adiabatic energy differences between the states.

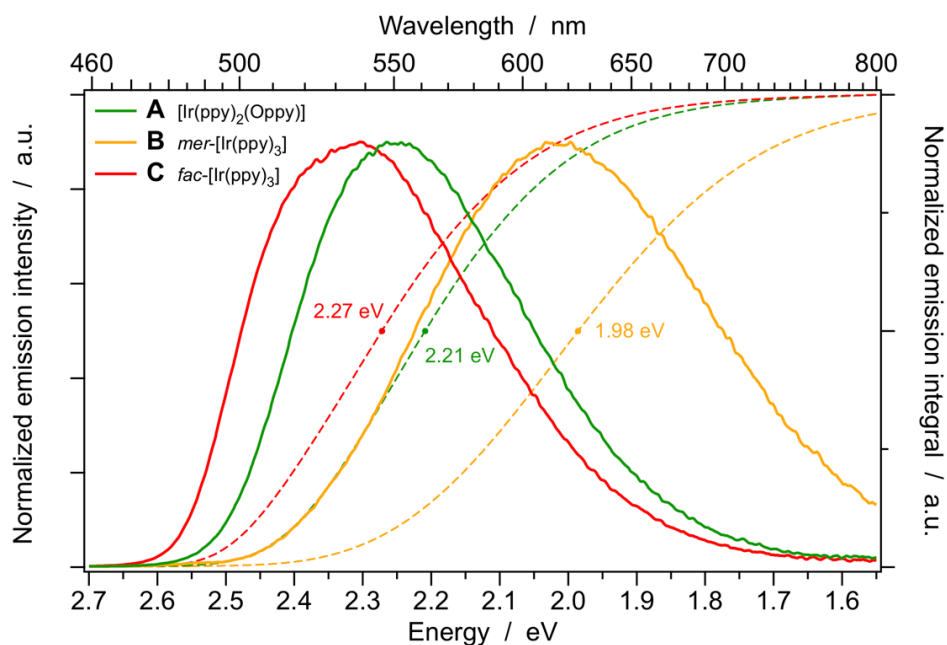


**Fig. S26** Corrected emission spectra of **A–C** in room-temperature acetonitrile solution, reported in relative quanta per energy interval. The mean-phonon energy (indicated by the dots) is calculated as the energy value at which the emission integral reaches 50% of the overall emission.